

Dynamic Switching of Lateral Inhibition Spatial Patterns

Joshua Hawley¹, Paul Glendinning², Nancy Papalopulu¹, Ceris Manning¹,
and Veronica Biga¹

¹Faculty of Biology Medicine and Health, The University of Manchester, Manchester, UK
²Department of Mathematics, The University of Manchester, UK

August 8, 2022

Abstract

Hes genes are transcriptional repressors activated by Notch. In the developing mouse neural tissue, HES5 expression oscillates in neural progenitors [1] and is spatially organised in small clusters of cells with synchronised expression (microclusters). Furthermore, these microclusters are arranged with a spatial periodicity of 3-4 cells in the dorso-ventral axis and show regular switching between HES5 high/low expression on a longer time scale and larger amplitude than individual temporal oscillators [2]. However, our initial computational modelling of coupled HES5 could not explain these features of the experimental data. In this study, we provide theoretical results that address these issues with biologically pertinent additions.

Here, we report that extending Notch signalling to non-neighbouring progenitor cells is sufficient to generate spatial periodicity of the correct size. In addition, introducing a regular perturbation of Notch signalling by the emerging differentiating cells induces a temporal switching in the spatial pattern, which is longer than an individual cell's periodicity. Thus, with these two new mechanisms, a computational model delivers outputs that closely resemble the complex tissue-level HES5 dynamics.

Finally, we predict that such dynamic patterning spreads out differentiation events in space, complementing our previous findings whereby the local synchronisation controls the rate of differentiation.

Keywords— Lateral inhibition, dynamic switching, spatial pattern, Notch signalling, HES5, neural tube

1 Introduction

The developing neural tube is a densely packed pseudostratified neuroepithelium and starting from E10 in mouse, apically located progenitors called radial glial (RG) cells asymmetrically divide, detach from the apical wall, and migrate basally to generate differentiating neuronal cells (Figure 1A) [3, 4]. In specific dorsal-ventral regions of the neural tube, RG cells express the transcriptional repressor HES5 (Figure 1A&B), which maintains cells in a progenitor state by repressing proneural gene expression [5, 6, 7, 8, 9, 1]. HES5 expression is dependent on active Notch signalling which is a pathway that enables contacting cells to signal to each other. Notch signalling can either act to laterally induce expression between cells, or laterally inhibit, and this is dependent upon the ligand that is interacting with the Notch receptor. If Notch interacting cells express Jagged (1 or 2), then active Notch signalling in one cell will induce active Notch in neighbouring cells. On the other hand if cells express Delta (1 or 4), then active Notch signalling in one cell will lead to inhibition of active Notch signalling in neighbouring cells. There are further considerations to bear in mind such as cis-inhibition where Delta on the same cell binds to and blocks Notch from becoming activated, as is the case with the ligand Delta-3 or high levels of Delta-1/4 [10, 11]. In the ventral HES5 domain, the main Notch ligand expressed is Delta-1 [12] and so from here onwards, Notch signalling will refer to Notch-Delta-1 lateral inhibition (LI) (Figure 1C).

This study investigates HES5 expressed in the p0-p2 and pMN domains of the neural tube, which are distinct progenitor domains that give rise to different neuronal subtypes (Figure 1A) [13]. It was previously known that individual cells are capable of oscillatory HES5 dynamics due to transcriptional autoinhibition [14] with a temporal period of around 3.3h [1], which we will refer to as ultradian oscillations. Around 50% of cells in the HES5 domain are found to exhibit oscillatory behaviour and otherwise have aperiodic noisy expression [1]. Two recently uncovered key aspects of HES5 expression observed in *ex vivo* slices of neural tube are first, that within the p0-p2 domains, HES5 is expressed in clusters of similar expression (groups of 3-7 cells) and these are arranged regularly to form an average spatial period of 3-4 cells measured along the dorsal-ventral axis [2]. Second, the location of high and low expression is not fixed over time, with clusters of similarly expressing cells spending an average of around 8h in a high or low state before switching to the opposite state. The ultradian oscillations have a mean temporal period of 3.3h as well as a smaller amplitude than the observed 8h switching behaviour, indicating that ultradian oscillations alone are not responsible for the longer switching behaviour. Indeed, both noisy and oscillatory single-cell HES5 dynamics are found to be nested within the larger amplitude switching behaviour of the cells when looking at individual cell traces [2]. Specifically, the amplitude of the longer switching dynamics is approximately twice that of the ultradian amplitude as determined previously [1].

Most theoretical models of Notch LI produce stationary patterns where cells do not switch between high and low states once the spatial pattern has formed [15, 16, 17, 18, 19, 20, 21]. Some literature explores antiphase oscillations of downstream Notch genes between coupled cells, but this concerns ultradian oscillations only, rather than ultradian oscillations nested within a distinct larger amplitude, longer time scale switching behaviour [22, 23]. Therefore the dynamic switching behaviour of the HES5 spatial pattern, as far as we are aware, is not accounted for in the literature. To simulate neural tube HES5 dynamics, Biga et al. used a multicellular Notch-HES5 model composed of parameterised single-cell dynamics that were coupled together via LI interactions, signalling only between closest neighbours (Figure 1D). This work considered that ultradian HES5 oscillations may interact via LI to generate an emergent behaviour similar to that observed in the neural tube. Aspects such as local synchronisation of HES5 dynamics could be reproduced, however other aspects of the data such as 3-4 cell spatial periodicity and larger amplitude temporal switching could not be reproduced, indicating that additional mechanisms are required to explain the observed patterns of dynamic behaviour.

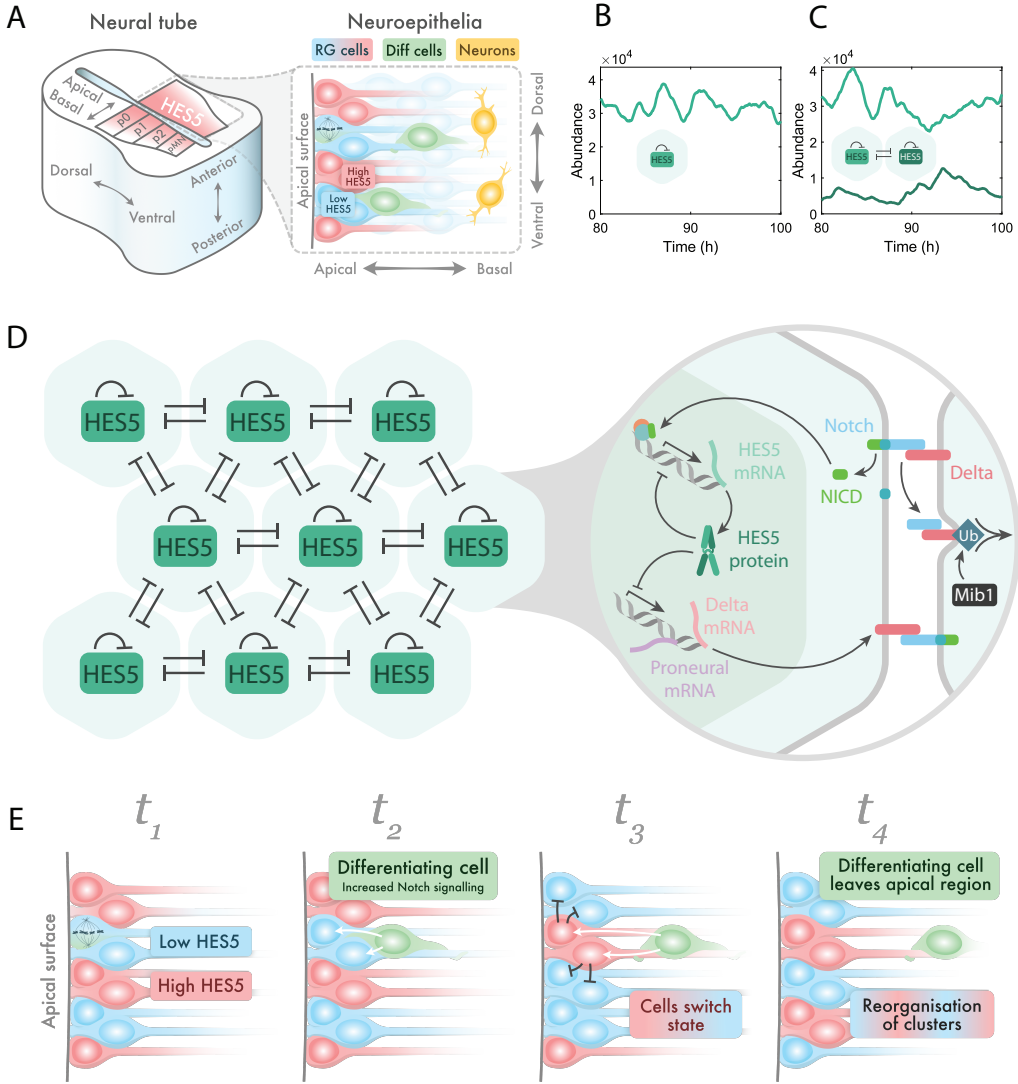


Figure 1: **A Left** Diagram of a neural tube cross section with domains p0-p2 and pMN highlighted which correspond to where HES5 is expressed. **Right** Structure of the neuroepithelium that makes up the neural tube, with various cell types highlighted. **B** Single-cell simulation time trace showing an example of HES5 autoinhibition producing noisy ultradian oscillations (single cell parameters in Table 1 were used to generate the time trace). **C** Time traces for a two-cell simulation with LI coupling (parameters in Table 1 used, $\tau_{LI} = 0$, and $P_{0,LI} = 4500$). **D Left** Hexagonal lattice summarising the interactions in the model which include nearest neighbour lateral inhibition and HES5 autoinhibition. **Right** Detailed interactions of the Notch-HES pathway which the modelling is based on. Abbreviations: Ubiquitination (Ub), Mindbomb1 (Mib1). **E** Shows the proposed mechanism by which differentiating cells could cause a reorganisation of the LI spatial pattern by increasing Notch activation in neighbouring cells. At time point t_1 , a spatial period is already present as a result of Notch signalling, and an individual cell is shown undergoing mitosis that will give rise to a differentiating cell in t_2 . At t_2 , a cell with low HES5 commits to differentiation and starts increasing both Delta and Mib1 expression. At t_3 , the increased signalling from the differentiating cell causes an increase in the amount of HES5 in the receiving cell, and the differentiating cell starts migrating basally. At t_4 , the differentiating cell eventually loses signalling contact with the RG cells at the apical surface, and a reorganised spatial pattern remains.

To understand the complexity and generation of the *ex vivo* neural tube pattern, we consider two new additions to the multicellular Notch-HES5 model presented in Biga et al.. The first addition is extending the LI signalling distance between cells, inspired by modelling work that shows how protrusions can extend Notch signalling distance which leads to longer period spatial patterns [18]. This is in line with experimental observations of filopodia in *Drosophila*, which have been shown to carry Notch ligands and induce Notch signalling several cell diameters away [17, 24], and various literature points to the existence of protrusions in the neuroepithelia that are likely capable of Notch signalling [25, 26, 27, 28]. The second addition to the model is the introduction of a differentiation process that alters the amount of Notch signalling that neighbouring cells receive from a differentiating cell. This process in the model is based on the fact that early differentiating cells migrating out of the RG population increase their expression of Delta [29] as well as Mindbomb1 (Mib1) which greatly increases the efficiency of Delta trans-activation of Notch [30, 31, 32]. Via ubiquitination, Mib1 marks Delta for endocytosis, which subsequently provides the mechanical force required for successful Notch receptor activation on neighbouring cells [30, 33] (Figure 1E).

To identify outputs similar to *ex vivo* dynamics in the new model, we use significance testing on power spectra to identify spatial periodicity and define a new measure, the dynamicity coefficient, to indicate the proportion of time cells spend in high and low states. By plotting these measured outputs in parameter space we identified that extended signalling distance generates spatial periods of 3-4 cells, and the inclusion of a differentiation process that dynamically alters signalling between cells produced switching behaviour between high and low HES5 expression over time. Additionally, the model output showed cases of ultradian oscillations nested within the larger amplitude, longer time-scale switching behaviour, as observed in single-cell data [2]. This is a unique exploration of how Notch LI signalling can be prevented from permanently settling into fixed peak and trough locations while maintaining the spatial pattern forming ability of LI. The reorganisation of peak and trough locations of HES5 over time is found to enable differentiation events to be spread out spatially over time and prevents hotspots where differentiating cells are repeatedly produced, potentially important in ensuring an even production of neurons across the dorsal-ventral axis.

2 Methods

2.1 Multicellular lateral inhibition HES5 model

Our core model is based on previously implemented modelling work, consisting of autoinhibition interactions of HES5 protein back on to expression of its own mRNA, and with HES5 dynamics being coupled between cells in a hexagonal geometry using an inhibitory Hill function representative of Notch LI [16, 34]. The single-cell parameters used in the model were previously parameterised to neural tube HES5 data using Bayesian inference [1], and a range of multicellular parameters were explored in [2]. Figure 1D outlines the biological interactions considered and the core interactions that are described mathematically in the model. A Chemical Langevin equation approach is used [35], and the stochastic delay differential equations that govern the dynamics of a cell at row i and column j (see Figure 2) in the multicellular model is given by

$$\frac{dm_{ij}(t)}{dt} = -\mu_m m_{ij}(t) + \alpha_m H_{auto}\left(p_{ij}(t - \tau_{auto})\right)H_{LI}\left(\bar{p}_{ij}(t - \tau_{LI})\right) + \eta_m, \quad (1)$$

$$\frac{dp_{ij}(t)}{dt} = -\mu_p p_{ij}(t) + \alpha_p m_{ij}(t) + \eta_p, \quad (2)$$

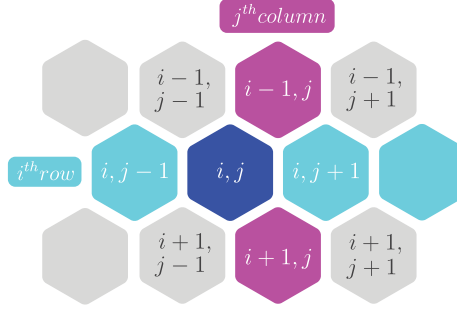


Figure 2: Indices in the model equations relate to the hexagonal geometry as shown.

where $m_{ij}(t)$ is HES5 mRNA concentration in the cell on the i^{th} row and j^{th} column at time t and $p_{ij}(t)$ is HES5 protein concentration. μ_m and μ_p are the degradation rates of HES5 mRNA and protein respectively, α_m and α_p are the transcription and translation rates respectively, τ_{auto} is the time delay associated with HES5 autorepression and τ_{LI} is the time delay associated with the lateral inhibition interaction between cells. In results section 3.2, we find that over a range of τ_{LI} values (0-100min), the model exhibited a similar behaviour. The somitogenesis literature points to a range of possible τ_{LI} values (20-120min), and so to reduce the complexity of the model we set $\tau_{LI} = 0$ for the main results, and give an exploration of non-zero time delays in the supplementary Figures S2 & S3 [36, 37, 38, 39, 40].

The functions H_{auto} and H_{LI} are both inhibitory functions that regulate mRNA production rate in response to protein abundance either within a cell (H_{auto}), or between cells (H_{LI}). H_{LI} therefore is the coupling function that enables HES5 dynamics to influence neighbouring HES5 dynamics. For the signalling contribution from each cell in contact with a receiving cell, we take the approach used in [16, 23], and the amount of HES5 a cell receives is the averaged abundance from all signalling neighbours

$$\bar{p}_{ij} = \frac{1}{|\mathcal{N}(i,j)|} \sum_{(i,j) \in \mathcal{N}(i,j)} \varepsilon_{i,j} p_{ij}, \quad (3)$$

where $\mathcal{N}(i,j)$ is the set of neighbours a cell is in signalling contact with and $|\mathcal{N}(i,j)|$ is the total number of neighbours in the set. Neighbouring cells are defined in Section 3.1 and this introduces proximal and distal cells. Proximal cells are adjacent cells, i.e. any neighbours within a 1-cell distance, and distal cells are signalling neighbours than lie further than 1-cell distance away (see Figure 6). Coupling strength of distal and proximal cells, ε_d and ε_p respectively, can be varied independently in the model and so $\varepsilon_{i,j}$ in equation (3) defines a coupling weighting dependent on whether the signalling neighbour is proximal or distal, and can have one of two values

$$\varepsilon_{i,j} = \begin{cases} 1, & \text{if } \mathcal{N}(i,j) \text{ is a proximal neighbour} \\ \frac{\varepsilon_d}{\varepsilon_p}, & \text{if } \mathcal{N}(i,j) \text{ is a distal neighbour} \end{cases} \quad (4)$$

The Hill functions are both decreasing functions where $H_{auto}(0) = H_{LI}(0) = 1$ and $H_{auto}(\infty) = H_{LI}(\infty) = 0$ and have the form

$$H_{auto}\left(p_{ij}(t - \tau_{auto})\right) = \frac{1}{1 + \left(p_{ij}(t - \tau_{auto})/P_{0,auto}\right)^{n_{auto}}}, \quad (5)$$

$$H_{LI}\left(\bar{p}_{ij}(t - \tau_{LI})\right) = \frac{1}{1 + \left(\bar{p}_{ij}(t - \tau_{LI})/P_{0,LI}\right)^{n_{LI}}}. \quad (6)$$

$P_{0,auto}$ and $P_{0,LI}$ are the repression thresholds of each Hill function. The repression threshold defines the amount of protein that results in a 50% reduction in mRNA production rate. For example, within an individual cell, the value of $P_{0,auto}$ defines the abundance of HES5 protein, p_{ij} , at which mRNA production rate will be 50% within that same cell. In the case of $P_{0,LI}$, this defines when mRNA production in a receiving cell will be 50% in response to the averaged incoming abundance of HES5 protein in the neighbouring cells \bar{p}_{ij} . n_{auto} and n_{LI} are the Hill coefficients which define how steep the gradient of the Hill function is at P_0 (higher values give a sharper transition between no repression and repression).

The terms η_m and η_p in equations 1 and 2, are the stochastic noise terms for mRNA and protein which are Gaussian white noise scaled by the square root of the number of events that occur in each process:

$$\eta_m = \sqrt{\mu_m m_{ij}(t) + \alpha_m H_{auto}\left(p_{ij}(t - \tau_{auto})\right) H_{LI}\left(\bar{p}_{ij}(t - \tau_{LI})\right)} \xi_m(t), \quad (7)$$

$$\eta_p = \sqrt{\mu_p p_{ij}(t) + \alpha_p m_{ij}(t)} \xi_p(t), \quad (8)$$

where $\xi_m(t)$ and $\xi_p(t)$ are Gaussian white noise with mean of 0 and variance of 1. Equations are solved using the Euler-Maruyama method, implemented in MATLAB. Model parameters are summarised in Table 1.

Table 1: Model parameter values used [2]

| Symbol | Value | Biological definition |
|---------------|------------------------------|---|
| a_m | 0.77 min^{-1} | Transcription rate |
| a_p | 26 min^{-1} | Translation rate |
| u_m | $\ln(2)/30 \text{ min}^{-1}$ | mRNA degradation rate |
| u_p | $\ln(2)/90 \text{ min}^{-1}$ | Protein degradation rate |
| $P_{0,auto}$ | 25,000 proteins | HES5 auto-inhibition repression threshold |
| $P_{0,LI}$ | 0-10,000 proteins | LI coupling repression threshold |
| n_{auto} | 3.5 | HES5 auto-inhibition Hill coefficient |
| n_{LI} | 3 | Lateral inhibition Hill coefficient |
| τ_{auto} | 30 mins | HES5 self-repression time delay |
| τ_{LI} | 0-100 mins | Lateral inhibition time delay |

2.2 Extracting spatial signals from the model

To understand what sort of spatial patterns are being produced by the model, we extract spatial signals using a similar approach to that used for the *ex vivo* analysis in [2]. In the hexagonal grid of cells, $p(x_{i,j}, t_k) = p_{ij}(t_k)$, denotes the protein expression at the i^{th} row, j^{th} column, and k^{th} time-step, and I, J, K are the total number of rows, columns, and time-steps. In the case of simulating a single column of cells ($J = 1$) such as in Figure 3A, a spatial signal can be generated for each time point by taking the protein expression along the entire column such that the spatial signal at time-step k and $j = 1$ is

$$S_k(x) = p(x_{1:I,1}, t_k). \quad (9)$$

Each spatial signal is therefore a vector of length I where each entry is the expression from an individual cell, and the total number of spatial signals that can be generated from a single simulation is $N_s = K$ (Figure 3B). To visualise both spatial and temporal aspects of the data in one plot, the spatial signal can be plotted over a range of time points $S_{k_1:k_2}(x)$ as a kymograph, shown in Figure 3A&C.

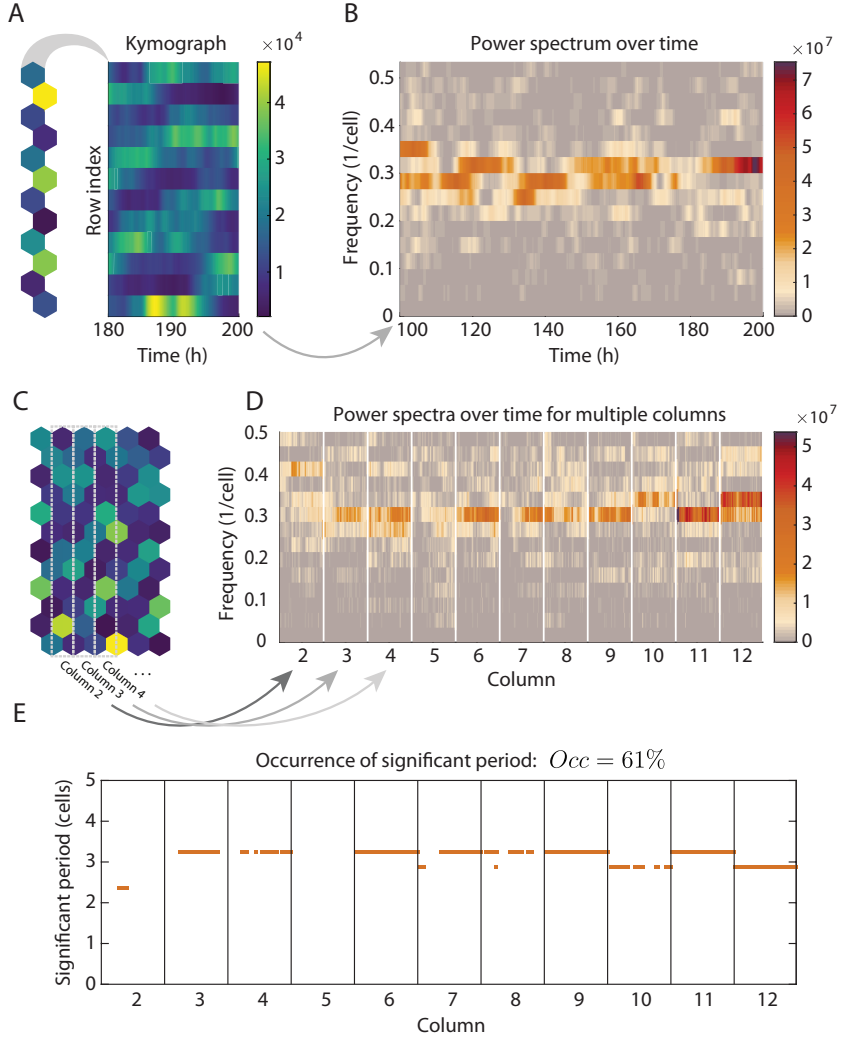


Figure 3: Outline of the process used for detecting the presence of significant periodic spatial patterns. **A** In the case of 1D simulations, kymographs are generated from the expression on each row (y-axis) and over time (x-axis). **B** A Fourier transform of the spatial signal in **A** is shown as a power spectrum over time, where colour indicates the power contribution of each frequency at each time point. **C** For 2D simulations, spatial signals are generated from the cells that fall within selection regions (grey dashed boxes). **D** A power spectrum is generated for the spatial signal in each column (within each division the power spectrum over time is given, like in **B**). **E** The peaks of each individual power spectra are tested for significance using the Fisher g -test (Methods section 2.3) and the significant spatial periods are plotted with orange dots and the occurrence measure is shown above the plot (Occ is defined in Methods section 2.3).

In the case of simulating multiple columns (i.e. a 2D grid of cells), we extract the spatial signal by using a selection region with a width of 1 cell and length I cells (see grey dashed boxes in Figure 3C). Due to the hexagonal geometry, on the even rows, two cells fall within this selection region and so the spatial signal is constructed as

$$S_{jk}(x_i) = \begin{cases} p(x_{i,j}, t_k), & \text{if } i \text{ odd} \\ \frac{p(x_{i,j}, t_k) + p(x_{i,j-1}, t_k)}{2}, & \text{if } i \text{ even} \end{cases} \quad (10)$$

where even rows use the average of the two cells that fall within the selection region. As there are multiple columns the number of spatial signals generated from a single simulation is $N_s = K(J - 1)$ (Figure 3D).

2.3 Detecting spatial periodicity

From the extracted spatial signals, a method is needed to detect the presence of statistically significant spatial periodicity in the inherently noisy model outputs. Using a fast Fourier transform method (MATLAB), a power spectrum can be obtained for each spatial signal

$$\mathcal{P}(S_{jk}(x)) = |\mathcal{F}(S_{jk}(x))|^2, \quad (11)$$

where $\mathcal{F}(S_{jk}(x))$ is the Fourier transform of the spatial signal. The highest power frequency in the power spectrum indicates the dominant periodicity in the spatial signal (Figure 3B&D). To distinguish if the detected peak is due to noise or genuine periodicity, a Fisher's g -test is implemented which compares the peak value in the power spectrum with the sum of the whole power spectrum and is defined as

$$g = \frac{\mathcal{P}(\omega_{peak})}{\sum_{n=1}^{N/2} \mathcal{P}(\omega_n)}, \quad (12)$$

where $\mathcal{P}(\omega_n)$ is the power/contribution from the n^{th} frequency ω analysed in the Fourier transform. The g -value tends to 1 in the case of genuine periodic signals, and 0 for noisy/aperiodic signals. To determine significance, a p-value can be calculated by comparing the likelihood of obtaining a higher g -value than the observed g if the power spectrum was generated from a purely noisy signal $S_\xi(x)$. This formally would be

$$p_{val} = P(g_\xi > g | H_0), \quad (13)$$

where g_ξ is the expected g -value obtained from $S_\xi(x)$, and H_0 is the null hypothesis. In this case, the null hypothesis is that the power spectrum is generated by Gaussian white noise, for which an analytical calculation of $P(g_\xi > g | H_0)$ is given in [41, 42]. Spatial signals with $p_{val} < 0.05$ are accepted as having significant periodicity present. Additionally, we define occurrence to be the fraction of all the spatial signals analysed (over all columns over all time points) that are found to have significant periodicity

$$Occ = \frac{N_s^{p_{val} < 0.05}}{N_s}. \quad (14)$$

Figure 3E shows an example of the significant periods detected in a 2D simulation, with the Occ value given.

2.4 Distinguishing dynamic and stationary spatial patterns

To develop a mathematical measure of how stationary or dynamic a pattern is over time, the dynamicity coefficient is defined here, which measures the proportion of time the expression in an individual cell spends in a high versus low state.

The choice of threshold that defines high and low states for the dynamicity measure is driven by our desire to analyse the dynamics at all levels of expression. As coupling strength is increased the mean expression is reduced, but the signal is still dynamic. Therefore, an absolute threshold cannot be used to measure dynamicity across a range of parameters. Instead, we define a relative threshold for each simulation by using the mean population expression level to ensure the threshold lies between the high and low states generated by lateral inhibition. While this ensures a high and low state is always defined, it comes with the caveat that when LI is too weak to produce distinct states, the dynamicity coefficient is reflecting switches due to the noisy fluctuations and ultradian oscillations of HES5.

The amount of time spent in an individual high or low state, which we call persistence time, is denoted by $T_{\uparrow,n}$ and $T_{\downarrow,n}$ respectively, where n is the n^{th} occurrence of a high or low state (see Figure 4A). Therefore the proportion of time a cell spends in a high state in a signal of length T_M (the measurement time) is

$$\alpha_{\uparrow} = \frac{1}{T_M} \sum_{n=1}^N T_{\uparrow,n}, \quad (15)$$

where N is the total number of occurrences of the cell being in a high state. Similarly, the proportion of the measurement time that a cell spends in a low state is

$$\alpha_{\downarrow} = \frac{1}{T_M} \sum_{n=1}^N T_{\downarrow,n}. \quad (16)$$

As α_{\uparrow} and α_{\downarrow} are proportions of the total measurement time, their values lie between 0 and 1, and $\alpha_{\uparrow} + \alpha_{\downarrow} = 1$. If $\alpha_{\uparrow} = \alpha_{\downarrow} = 0.5$, then this implies that an individual cell spends equal amounts of time in high and low states. In the opposite case where either $\alpha_{\uparrow} = 1$ and $\alpha_{\downarrow} = 0$, or $\alpha_{\uparrow} = 0$ and $\alpha_{\downarrow} = 1$, this implies that the cell spends the entire measurement time in one state, and therefore is classed as a stationary signal (Figure 4B). Using these proportions of time spent in high and low states, we define here the dynamicity coefficient as

$$D_c = 2 \times \min(\alpha_{\uparrow}, \alpha_{\downarrow}), \quad (17)$$

which rescales the proportions to give a value between 0 and 1; 0 if the signal/patterning is stationary, and 1 when the signal spends equal amounts of time in the high and low state ($\alpha_{\uparrow} = \alpha_{\downarrow} = 0.5$). To prevent transient fluctuations above or below the population mean contributing to the α_{\uparrow} , α_{\downarrow} values, a Savitzky–Golay filter (inbuilt MATLAB function) was used to smooth the signal first, using polynomial order of 1 and frame length of 165 minutes [43].

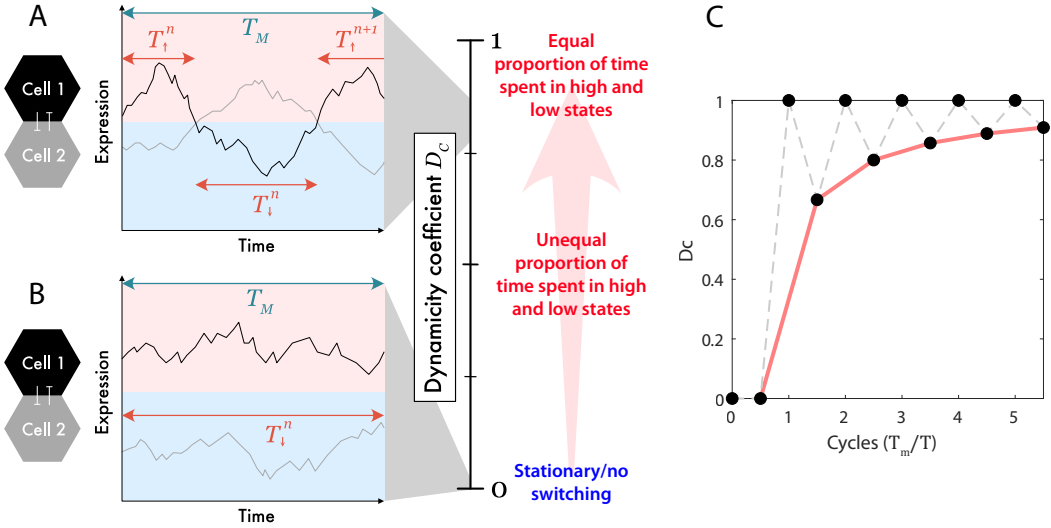


Figure 4: Illustrative examples and plot of the dynamicity coefficient. T_M is defined as the total measurement time/the length of the signal analysed and $T_{\uparrow,\downarrow}^n$ denotes the time spent above or below the mean population expression. **A** Plot of expression in two individual cells (black and grey) that exhibit dynamic LI where each cell can switch between a high state (pink upper half of the graph) and low state (lower pale blue half). **A** Corresponds to a high D_c value. **B** Two cells exhibiting a stationary LI interaction where one cell remains high (black) and one cell remains low (grey) over the whole measurement time. **B** corresponds to $D_c = 0$. **C** D_c values that would be obtained for a perfectly switching (regular period) signal at integer and half-cycles (black dots). Half cycle measurements are joined with a red line.

Another property that is useful to extract from the data is how frequently cells switch between high and low states. Here we define the persistence time as how long the signal persists in a high or low state, which is just the mean time spent high or low

$$\bar{T}_{\uparrow} = \frac{1}{N} \sum_{n=1}^N T_{\uparrow,n}. \quad (18)$$

$$\bar{T}_{\downarrow} = \frac{1}{N} \sum_{n=1}^N T_{\downarrow,n}. \quad (19)$$

In the case of regular temporal switching between states i.e, an oscillator with a well defined, non-varying period, then the period of the oscillator is given by $T = \bar{T}_{\uparrow} + \bar{T}_{\downarrow}$.

Note that the measurement time, T_M , will affect the D_c value to some extent, depending on how comparable T_M is to the expected period of switching T . Take for example a perfectly switching signal where $\alpha_{\uparrow} = \alpha_{\downarrow} = 0.5$, if we define the number of measured cycles $n_c = T_m/T$, then when n_c is integer, $D_c = 1$. However when the measurement time does not coincide with a full cycle, i.e. n_c is non-integer, then $D_c < 1$, because $\alpha_{\uparrow} \neq \alpha_{\downarrow}$. α_{\uparrow} and α_{\downarrow} will be most different and therefore D_c values will reach a minimum at half cycles and for a perfectly switching signal the D_c value at half cycles ($n_c = 0.5, 1.5, 2.5, \dots$) is

$$D_c = \frac{2(n_c - \frac{1}{2})}{2(n_c - \frac{1}{2}) + 1}, \quad (20)$$

This effect of measurement time cutting off at non-integer cycles only becomes a significant

issue when n_c is on the order of a few cycles and so the longer the measurement time relative to the switching period, the more accurate the D_c value becomes (see Figure 4C).

2.5 Implementation of the differentiation-based perturbation algorithm

To implement a process in the model that represents the signalling strength changes due to cell differentiation, we first require a process to determine the locations of differentiating cells and then a process to apply a changed signalling strength to the area around the differentiating cell. For differentiation, we make use of our previously developed differentiation algorithm [2]. This decision process is based on the assumption that lower levels of HES5 are more likely to enable the upregulation of proneural genes, and therefore cells are marked for differentiation in a probabilistic manner based on expression (Figure 5A). Probability of a given cell to be marked for differentiation is given by

$$P(\text{diff} | p_{ij}(t)) = \begin{cases} 0, & p_{ij}(t) > D_{\text{thresh}} \\ R \left(\frac{D_{\text{thresh}} - p_{ij}(t)}{D_{\text{thresh}}} \right), & p_{ij}(t) < D_{\text{thresh}} \end{cases} \quad (21)$$

where D_{thresh} is the differentiation threshold (set as the population mean expression), and R is the rate of differentiation. For further details on the differentiation algorithm, see [2].

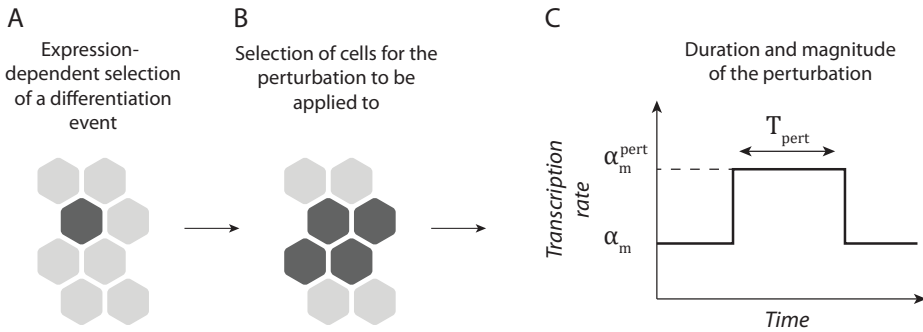


Figure 5: Outline of the DBP algorithm. **A** The probability-dependent differentiation algorithm is used to first identify a region where a cell is most likely to differentiate (single dark grey hexagon) based on HES5 expression levels (equation (21)). **B** An area around the selected cell in **A** is then selected (4 dark grey hexagons), and these cells will have the perturbation applied to the HES5 transcription rate with magnitude $F_{\text{pert}} = \frac{\alpha_m^{\text{pert}}}{\alpha_m}$ for a period T_{pert} shown in **C**.

In the neural tube, differentiating cells delaminate from the apical side in a process called apical abscission [4], and migrate outward towards the basal side [44]. However, cell movement is not modelled here and so differentiation events have to represent something less than the full picture of cell differentiation. Here we model the effects of a changed signalling strength coming from a differentiating cell in a given area, rather than simulating the differentiating cell explicitly as a separate cell. This involves choosing a number of cells around the area of the already selected differentiation location that are defined to be in contact with a differentiating cell in that area (Figure 5B). A perturbation is then applied to the HES5 transcription rate, α_m , in these cells to reflect increased Notch activation in these cells (Figure 5C). The magnitude of the perturbation applied to α_m is determined by a perturbation factor F_{pert} , so the perturbed HES5 transcription rate is α_m^{pert} where

$$\alpha_m^{\text{pert}} = F_{\text{pert}} \alpha_m. \quad (22)$$

Finally, a period of time for the perturbation to be applied is denoted by T_{pert} (Figure 5C). Values for T_{pert} and F_{pert} are discussed in section 2.5.

In the single column simulation, if cell i is the location where a differentiation event is chosen, then the perturbation is applied to both cell i and with equal probability either cell $i - 1$ or $i + 1$. If it is a grid simulation, then the perturbation is applied to a group of 4 cells: always i, j and $i, j + 1$ and then either the two cells above ($i - 1, j$ and $i - 1, j + 1$) or below ($i + 1, j$ and $i + 1, j + 1$). The entire process described in this section is referred to as the differentiation based perturbation (DBP) algorithm.

Differentiation rates in the simulations are characterised in two different ways. First, the average rate of differentiation over the whole population is calculated as the number of differentiation events that occur per hour as a percentage of the total number of cells in the simulation. Second, to look at how differentiation rates vary in individual cells, the frequency of differentiation per cell is calculated as the number of differentiation events per hour for every cell and then the distribution can be visualised in a histogram (Figure 10D-F).

3 Results

3.1 Extended signalling distance generates the correct spatial periodicity

Previous work found that the largest spatial period that can be generated from a HES5-Notch model with nearest-neighbour coupling is a 2-cell period of alternating high and low expression shown in Figure 6A-C [2]. However, HES5 expression in the neural tube exhibits clusters of similarly expressing cells that are arranged to generate a higher spatial periodicity of 3-4 cells, therefore an additional mechanism is required. Given that extending Notch signalling distance has been shown to enable longer spatial periodicity [45, 18, 46], and protrusions have been observed in many neuroepithelial tissues [17, 25, 26, 27, 28], we add *distal* cell interactions to represent the longer-range protrusion-based signalling (Figure 6D-F).

The distal geometry shown in 6D was found to generate sufficiently clustered patterns of the correct spatial period of 3-4 cells (Figure 6E&F) whereby groups of neighbouring cells form areas of high or low expression. In the 1D case (Figure 6E), distal cell interactions enable a clear alternating pattern of 2 cells high and 2 cells low. In the 2D case (Figure 6F), the periodic repeating also extends in the second dimension, and a mixture of cluster sizes can be seen in Figure 6F.

HES5 clusters *ex vivo* are composed of 3-7 cells on average and are elongated in the apical-basal direction [2]. Though no quantification is done on cluster size in this model, the high expressing clusters can be seen to be more on the order of 2-4 cells in size in 6F. The cluster sizes being lower than *ex vivo* measurement is likely due to there being no elongation of clusters in the model, and it is not known what causes the elongation *ex vivo*. Despite the apical-basal elongation not being reproduced, the dorsal-ventral spatial period of 3-4 cells is reproduced in the model, which is shown in the spatial period analysis in Figure 7&8. Other distal geometries were explored and simulations with higher numbers of neighbours produced less clustered or less robust patterns (Supplementary Figure S1). For all subsequent simulations, the distal geometry shown in 6D is used.

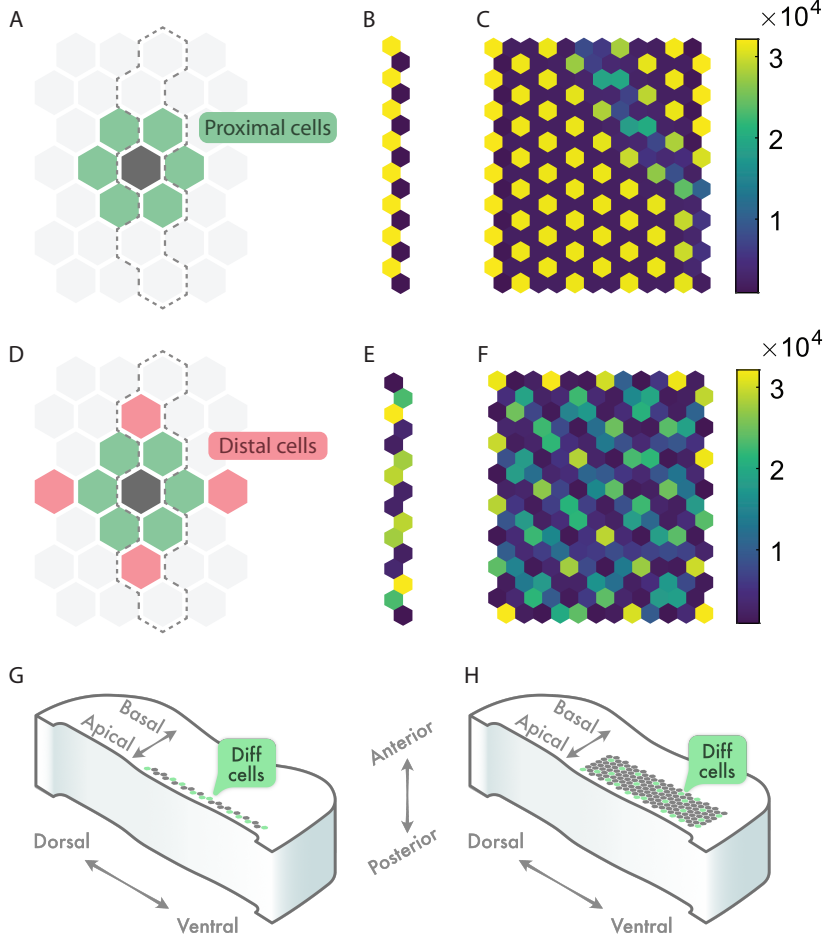


Figure 6: Comparison of deterministic model outputs with and without distal cells (**A-F**), and the mapping of the model lattice to the neural tube (**G&H**). **A** shows a cell (dark grey) and the cells it is coupled to in a hexagonal grid in the case when only proximal cells (green) are considered, and the dashed outline indicates the interactions included for 1D simulations. **B** and **C** show the final time point (200h simulation) of a 1D and 2D simulation respectively using the interactions shown in **A**. **D** shows the extended interactions used for all subsequent simulations, which includes the distal cells (red) in addition to the proximal cells (green). **E** and **F** show the final time point (200h simulation) of a 1D and 2D simulation, using $\frac{\varepsilon_d}{\varepsilon_p} = 1.5$. All simulations shown used $P_{0,L1} = 4000$. **G** The 1D lattice represents a line of cells in the dorsal-ventral direction towards the apical side of the tissue. Green cells indicate differentiating cells. **H** The 2D model lattice maps to the dorsal-ventral, apical-basal plane of the tissue.

Inspired by modelling work done by [18], proximal and distal signalling strength can be varied relative to each other and distal signalling efficiency here is given by $\frac{\varepsilon_d}{\varepsilon_p}$, where ε_d is the distal coupling strength (ND repression threshold) and ε_p is the proximal coupling strength. The effect of distal signalling efficiency is explored in the next section.

The 1D simulations represent a strip of cells in the dorso-ventral direction in the neural tube, towards the apical side where progenitor cells are located and differentiating cells are born (Figure 6G). The 2D simulations map on to a dorsal-ventral, apical-basal plane (Figure 6H). In both cases, this is to match the location of the HES5 domain and the axes that have been studied experimentally. In results section 3.3, differentiating cells are allowed to appear anywhere in the 2D lattice, and so for the dorsal-ventral, anterior-posterior plane assumption to make sense, differentiating cells would need to be distributed across the apical-

basal direction of the HES5 domain *ex vivo*. This is likely the case, as differentiating are born in the apical domain and subsequently migrate basally (as illustrated in Figure 1E), and so will likely contact a number of different cells throughout the apical-basal axis. If this is not the case and differentiating cells have a spatial distribution in a particular apical-basal area, then future work could look at the effects of restricting where these differentiating cells appear in the model.

3.2 Differentiation expands the dynamic patterning regime in 1D simulations

In addition to the periodic expression of 3-4 cells, the clusters of similar expression exhibit dynamic switching between high and low expression *ex vivo*. The DBP algorithm described in Methods 2.5 outlined the process through which differentiating cells perturb neighbouring progenitor cells through altered signalling strength. We present the model both with and without the DBP algorithm included to compare which model is more consistent with the dynamic switching observed *ex vivo*. This first set of results uses 1D simulations of 26 rows by 1 column, as this roughly matches the number nuclei within the dorsal-ventral HES5 expression domain (Figure 6G) as seen in [2].

To analyse the output of the model, three measurements were plotted in parameter space of distal signalling efficiency ($\frac{\varepsilon_d}{\varepsilon_p}$), versus the LI repression threshold (the coupling strength between cells) (Figure 7). Without DBP (Figure 7A), the spatial period tends towards 2 cells at zero/low distal signalling efficiency and towards higher periodicity as distal signalling increases. Occurrence of a significant spatial period (Methods 2.3) becomes more likely at lower repression threshold values (stronger coupling strength). However as occurrence increases, the D_c value decreases, indicating that the spatial patterns forming are largely stationary ones.

Regions of the parameter space are defined to be a good match to the experimental observations and exhibit dynamic spatial patterns if the spatial period, $T_{spatial}$, occurrence Occ , and dynamicity coefficient D_c satisfy

$$T_{spatial} > 3, \quad Occ > 0.4, \quad \text{and} \quad D_c > 0.4. \quad (23)$$

Despite the DBP algorithm not being present, there are perturbations due to expression noise and the ultradian oscillations. It is these inherent variations in expression that cause the thin dynamic pattern region of parameter space in Figure 7B, when the coupling strength is sufficiently strong to induce a weak spatial pattern, but weak enough for the inherent perturbations to enable dynamic switching between high and low states. See Supplementary Movie 1 for an animated 1D simulation without DBP included.

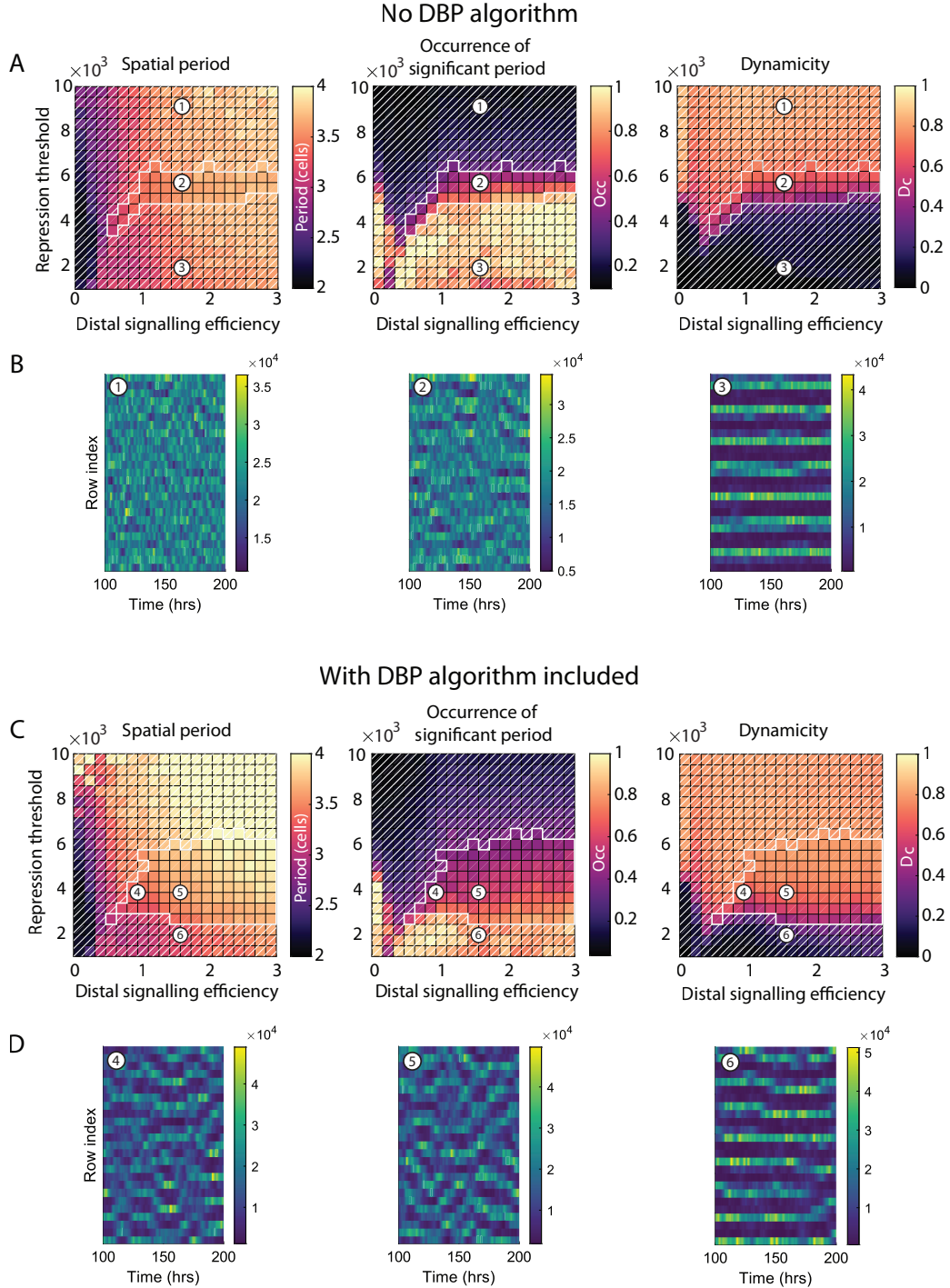


Figure 7: Simulations of a single column of cells (26 rows, 1 column). Parameter space values were generated by taking the mean value from 20 simulations with random initial conditions. The top two rows show model output without the DBP algorithm, and the bottom two rows show the output with DBP included. Rows **A** and **C**: Parameter spaces show distal signalling efficiency, $\frac{\varepsilon_d}{\varepsilon_p}$, versus lateral inhibition repression threshold, $P_{0,LI}$, and three different measured model outputs are indicated by the colour-scale. Areas without white diagonal lines overlaid indicate regions that satisfy equation (23) ($T_{spatial} > 3$, $Occ > 0.4$, $D_c > 0.4$), which is where dynamic spatial patterns occur. **Figure legend continues on next page.**

Figure 7: **Left** Spatial period where only statistically significant periods are plotted (see methods section 2.3). **Middle** Occurrence of significant spatial period (see methods section 3). **Right** Shows the dynamicity measure (see methods 4). Rows **B** and **D**: Example kymograph plots from corresponding numbered regions in parameter space. Kymographs used the following parameters: 1) $P_{0,LI} = 9053$, $\frac{\varepsilon_d}{\varepsilon_p} = 1.58$, 2) $P_{0,LI} = 5737$, $\frac{\varepsilon_d}{\varepsilon_p} = 1.58$, 3) $P_{0,LI} = 1947$, $\frac{\varepsilon_d}{\varepsilon_p} = 1.58$, 4) $P_{0,LI} = 3842$, $\frac{\varepsilon_d}{\varepsilon_p} = 0.95$, 5) $P_{0,LI} = 3842$, $\frac{\varepsilon_d}{\varepsilon_p} = 1.58$, 6) $P_{0,LI} = 1947$, $\frac{\varepsilon_d}{\varepsilon_p} = 1.58$.

For simulations that include the DBP algorithm, we estimated values for T_{pert} and F_{pert} from the literature. Experimental work in chick neural tube found that Tis21, a marker for neurogenically dividing neural progenitors, was upregulated around 8h after Delta-1 was expressed in the same cell, followed by the generation of neurons around 16h [47]. Assuming that within this time, signalling from the Delta-1 expressing cell upregulates Notch signalling in neighbouring cells, then at least 8h perturbation seems reasonable, and we choose a value of $T_{pert} = 7h$. In Supplementary Figure S2 & S3, an exploration of other T_{pert} values found that longer perturbation enhanced the range of parameters in which dynamic patterning occurred. To estimate a value for F_{pert} , we searched for literature that explores upregulation of Mib1 and its effect on neighbouring cell's Notch response, as Mib1 determines the efficiency of trans-activation of Notch signalling. One study looked at the effect of co-culturing mouse neocortex Mib1 positive intermediate progenitors and Mib1 negative RG cells with Notch1 expressing cells and compared the resulting levels of Hes1 expression within these Notch1 cells [31]. Two methods were used to isolate populations of Mib1 positive cells, and it was found that compared to RG cells, Mib1 positive cells caused between a 1.8-3.7 fold increase in Hes1 expression. In an *in vivo* study of chick neural tube, upregulation of both Delta-1 and membrane localised Mib1 caused a 1.8 fold increase in HES5 intensity in RG cells [32]. We chose a value from the higher range of these Mib1-induced increases in HES and set $F_{pert} = 3$.

With the DBP algorithm included in the simulation (Figure 7C&D), the parameter space for spatial period and occurrence remains broadly similar. However, high D_c values extend further into lower repression thresholds (high coupling strength) when compared to the simulations without DBP (Figure 7A&B). This generates an expanded region of parameter space that satisfies equation (23) (region without white diagonal lines overlaid in Figure 7C). The kymographs D(4) and (5) further confirm and visualise how the dynamic pattern evolves, showing a more definite and higher amplitude spatial pattern forming (compared with B(2)) but still with switching of peaks and troughs, and even some transient travelling wave type behaviour. At very low repression threshold D(6), stationary patterns still emerge when the perturbation strength cannot overcome the effects of strong coupling. See Supplementary Movie 2 for an animated 1D simulation with DBP included.

We explored the effect of varying the LI time delay between cells. The literature indicates a wide range of possible values this could take, from 20-120min [36, 37, 38, 39, 40], and in the supplementary Figure S2 & S3 τ_{LI} values between 0-100min are tested, along with T_{pert} values between 0-14h. The results show that as τ_{LI} increases, the dynamic patterning region decreases, but crucially the region still expands when DBP is included, indicating robustness of the proposed mechanism. This reduced dynamic patterning region at longer LI time delays can be expanded by increasing the duration of T_{pert} , which is the time that a differentiating cell exerts higher signalling on its neighbours. As the expanding effect of DBP inclusion was found to occur across all LI time delays, and due to uncertainty in the actual value of the time delay, we chose to reduce the complexity of the model for the main results and use a value of $\tau_{LI} = 0\text{min}$.

Taken together this set of results indicates that from the underlying stationary pattern formed by LI, the pattern can be made dynamic by the introduction of perturbations to HES5 levels. The perturbations drive individual cells away from the two attractor states generated by LI (higher/lower phenotype between signalling neighbours) and thus enable opportunities for the reorganisation of peak and trough locations. The ability to switch states is a balance

between coupling strength and perturbation size; at higher coupling strengths, the perturbations cannot change the abundance of HES5 enough to enable a switch between low/high abundance in their neighbours. Conversely, at weak coupling strength, the system has no spatial pattern forming ability. Between these extremes lies a region where lateral inhibition is strong enough to form spatial patterns if unperturbed but capable of switching states given sufficient perturbation.

3.3 Dynamic spatial patterning occurs in 2D simulations

To explore how introducing more signalling neighbours affects the dynamic pattern forming ability of the model, we simulate a 2D hexagonal grid and show that the 1D results of the previous section extend to the 2D case. A grid size of 26 rows by 6 columns is chosen as this corresponds approximately to the number of nuclei within the dorsal-ventral, apical-basal HES5 expression domain (Figure 6H) [2]. The 2D arrangement involves an additional 4 proximal and 2 distal neighbours compared to the 1D simulations, meaning that each cell receives an average input signal generated from a larger number of neighbours.

Without DBP included (Figure 8A), the parameter space outputs were generally similar to the 1D case (Figure 7A). However, the dynamicity was found to be largely low in the region where high occurrence of a spatial period was found, indicating that only stationary patterns can be generated. The absence of robust dynamic patterning is confirmed by the thin band where equation (23) is met (region without a white diagonal line overlay in Figure 8A), much smaller than in the 1D case. This appears to be due to the additional signalling from the higher number of cells (10 signalling neighbours in the 2D case versus 4 neighbours in the 1D case) which reinforce the strength of lateral inhibition, making switching states due to stochastic noise and HES5 oscillations less likely. Additionally at low repression threshold values/high coupling strength (0-2000 in Figure 8A), occurrence was found to be lower than in the 1D case. In this region, LI is found to still drive expression to high and low states as expected, however due to the higher number of neighbours, the increased signalling strength resulted in irregular patterns, causing a spread of frequency values in the power spectrum, and therefore no single significant peak detected using the Fisher *g*-test.

When the DBP algorithm is included (Figure 8B), dynamic patterning is recovered, and a region of high dynamicity is found to overlap with high occurrence of a spatial period. Comparing the acceptance region that satisfies equation (23) in Figure 8B to the 1D case in Figure 7D, it can be seen that the area is reduced and shifted slightly towards higher distal signalling efficiencies. Whereas in the 1D case where distal signalling efficiencies of 1 were found to generate dynamic patterning, the minimum efficiency required in 2D is $\frac{\varepsilon_d}{\varepsilon_p} > 1$. This need for higher distal signalling is due to the fact that when there are higher numbers of neighbours, individual cells contribute less of an effect on their neighbours, due to the incoming signal being the averaged expression of the neighbours. See Supplementary Movie 3 for an animated 2D simulation with DBP included.

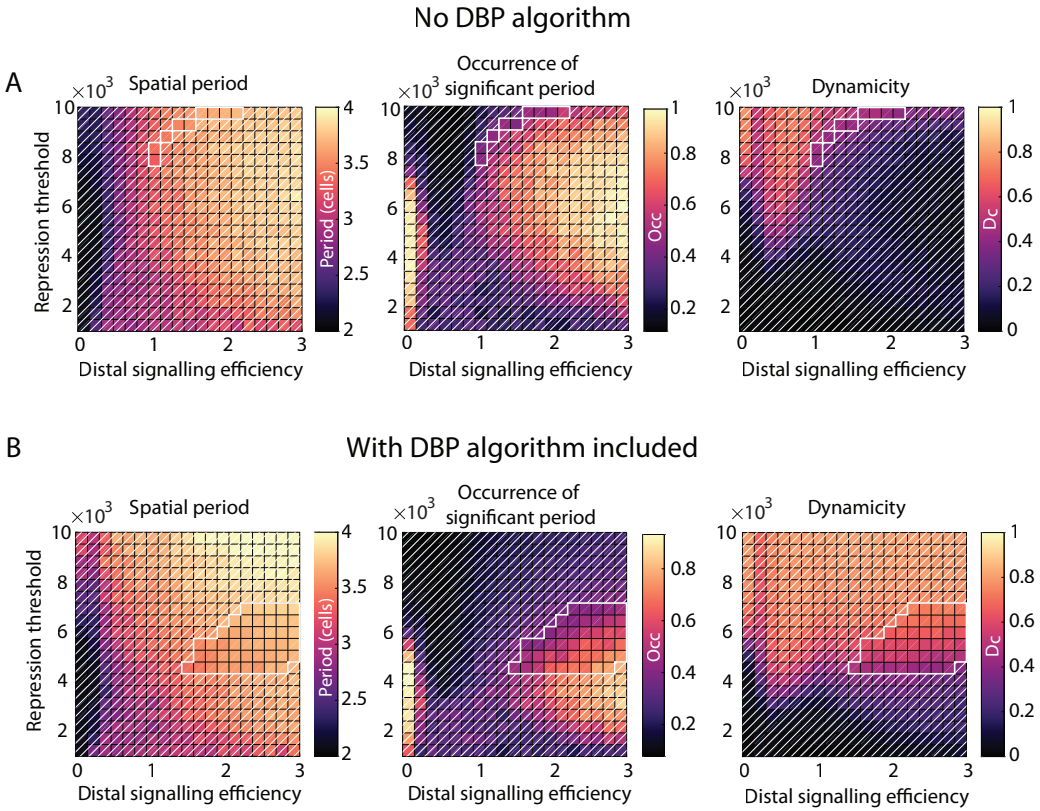


Figure 8: The same parameter spaces as in Figure 7 are plotted here but for 2D simulations (26 rows, 6 columns). Parameter space values were generated by taking the mean value from 20 simulations with random initial conditions. Row **A** shows model output when the DBP algorithm is not included, row **B** includes the DBP algorithm. Areas without white diagonal lines overlaid indicate regions that satisfy equation (23) (spatial period > 3 , occurrence of spatial period > 0.4 , and a dynamicity coefficient > 0.4), and where dynamic spatial patterns are expected to occur.

As protrusions have a much smaller contact area than when two cell bodies contact, one might intuitively expect more Notch signalling to occur at the cell body. However, one study identified that not only is contact area an important consideration, but that also the diffusion rate of Notch and Delta across the cell membrane influences the amount of signalling that occurs. Higher diffusion rates of Notch and Delta, likely enabled by active transport within protrusions, can in fact enable higher rates of Notch signalling in protrusions than in a larger contact area of cell body with lower diffusion rates of Notch/Delta [48]. In other modelling work, Hadjivasiliou et al. suggested the ability to mechanically pull on Delta and subsequently activate Notch signalling may be different at the cell body versus the protrusions [18]. They hypothesised this difference could be caused by either a reduced amount of endocytosis at the main cell would lead to less activation, or that the dynamic extending/retracting nature of protrusions could provide the mechanical force required for activation. A final possibility is that cis-inhibition may more common in the cell body than in protrusions, and this would occur if high amounts of both Notch and Delta are present on the cell body, but only one of Notch or Delta is found in the protrusions.

As discussed in the previous section, when DBP is not present in the 1D simulations, the noisy fluctuations and ultradian oscillations are capable of producing a thin region of parameter space where weak dynamic patterning can occur (Figure 7A). This prompts the question: to what extent do these smaller amplitude fluctuations affect switching when DBP is included?

Without DBP, dynamic patterning occurs at weaker LI coupling strengths, where the two high and low attractor states are not sufficiently attracting to prevent noise/ultradian oscillations from inducing switches between the two states. However, at stronger coupling strengths, the LI states attract more strongly, and make smaller amplitude fluctuations increasingly unlikely to induce switching between states when compared to the larger amplitude perturbations provided by DBP (Figure 7C and 8B). This does not rule out that noise/ultradian oscillations play some role in enhancing switching, but it is clear from this analysis these smaller amplitude fluctuations are not sufficient to induce switching at stronger coupling strengths.

3.4 Ultradian oscillations are nested within the larger amplitude DBP switching behaviour

Ex vivo observations from Biga et al. indicate that the temporal dynamics of single cells consists of both noisy and ultradian oscillations (average temporal period of 3.3h) nested within larger amplitude, longer time scale switching behaviour (average time spent high or low was 8h). Through measuring persistence times and plotting single-cell time traces, DBP is found to produce similar nested dynamics to that in the neural tube.

In addition to D_c values, persistence time gives useful information about which processes are contributing to any switching behaviour that is occurring. As defined in Methods 2.4, persistence time refers to the amount of time a cell spends in a high or low state before switching the opposite fate, and the distribution of low and high persistence times is plotted in Figure 9A-C ii. Noisy/ultradian dynamics are characterised by mean persistence times of around 3.6h-3.9h, as revealed by running the model without LI and without DBP (Figure 9A ii). These noisy/ultradian persistence times that make up the left-most parts of the distributions are found to be present in all model conditions (Figure 9A-C ii).

When LI coupling is included in the simulations, but DBP is not (Figure 9B ii), the distribution is shifted to longer persistence times than in the uncoupled case. The LI induces two larger amplitude high and low states (Figure 9B i), while maintaining smaller amplitude noisy/ultradian oscillations at the mean levels dictated by the LI. This results in noisy/ultradian dynamics not being able to contribute to the switching as much, and the mean persistence times are longer at 27.3-30.9h. Additionally a peak at 150h is found (Figure 9B ii), which means that a fraction of the cells spend the entire measurement time stuck in one state, indicating more stationary patterning.

Crucially, the inclusion of DBP into the LI model (Figure 9C) removes the peak at 150h, while still maintaining longer mean persistence times (10.8-12.9h) than the uncoupled model. The single-cell time trace in Figure 9C i, shows a more regular switching than in B i, while still being distinct from the shorter timescale ultradian oscillations in A i. Relating this back to the observation of nested dynamics in [2], it can be seen that a similar nested oscillation behaviour occurs in the model with DBP included (Figure 9C i), with a mixture of smaller amplitude noisy dynamics and ultradian oscillations (red arrows in 9C i) being nested within the larger amplitude switching dynamics generated by the LI and DBP algorithm.

While there is more regularity in the switching in 9C than in A or B, the distribution still has a wide spread of possible persistence times in C ii. The *ex vivo* observations are limited to measurement times of at most 16h, and the mean experimental persistence times indicated a tighter distribution with a mean value of around 8h. While inclusion of DBP in the model fits the data closest, further exploration is needed to understand how the persistence time distributions can be made tighter in line with the *ex vivo* observations.

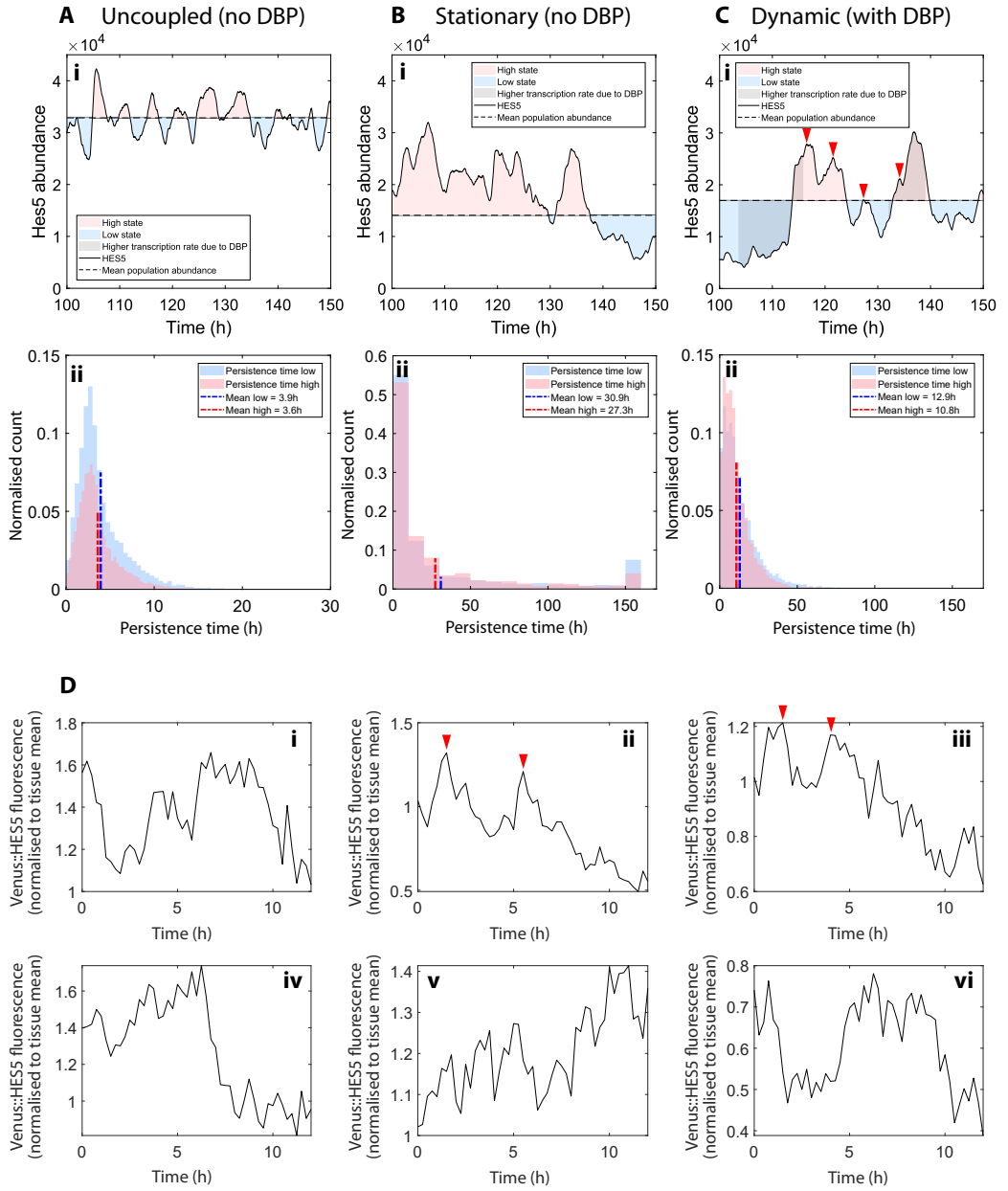


Figure 9: Top row (i) shows representative single-cell time traces, (ii) shows histograms of individual persistence times $T_{\uparrow,n}$ (pink), and $T_{\downarrow,n}$ (blue) (see Methods 2.4 for a definition of persistence times). Column **A** is the model output with no DBP algorithm included and no LI coupling between the cells. Column **B** is the model output with no DBP algorithm included and $P_{0,LI} = 4000$. Column **C** is the model output with DBP algorithm included and $P_{0,LI} = 4000$, red arrows indicate peaks in ultradian oscillations. Simulations in **i** used 1 column, 26 rows, and simulation run time of 200h. **ii** Data from 30 individual simulations plotted. Each simulation used 26 rows, 1 column, simulation run time of 300h and only the last 150h of the simulation was used to measure persistence time. **D i-vi** Single cell Venus::HES5 fluorescence time traces taken from experiment source data in [1] and replotted here.

For a visual comparison between the model with DBP (Figure 9C **i**) and the experimental data, single-cell time traces are plotted in Figure 9D **i-vi** which show Venus::HES5 fluorescent intensities tracked over 12h (replotted from source data in [1]). These traces are limited to

12h due to experimental constraints, much shorter than the plotted simulation outputs, and so at most show two switches between high and low states (Figure 9D **i** & **vi**). Both high-to-low and low-to-high switches are observed in the experimental data, with a mix of aperiodic and period dynamics observed. Figure 9D **ii** & **iii**) show more pronounced transient ultradian oscillations which then become aperiodic noisy expression at later time points (red arrows indicate peaks of ultradian dynamics). Importantly the amplitude (peak to trough difference in fluorescence) is smaller in the ultradian oscillations than in the longer term switching behaviour of the single-cells, and previous analysis found that the longer term trend has an amplitude (standard deviation of normalised HES5 expression levels) approximately twice that of the ultradian oscillations [1]. Though not quantified here, it can be seen in Figure 9C **i** that the ratio of longer switching to ultradian oscillation amplitude is of the same order as the experimental data.

3.5 Dynamic patterning spreads out differentiation events spatially while maintaining a higher differentiation rate than the uncoupled model

To explore the potential functionality of the dynamic patterning, the spatial distribution of differentiation events and the rate of differentiation was explored by comparing 3 different conditions: a stationary spatial pattern (Figure 10A&D), a dynamic spatial pattern (Figure 10B&E), and no spatial pattern via uncoupled cells (Figure 10C&F).

To visualise how patterning affects the spatial aspect of differentiation, bar graphs showing the total number of differentiation events that occurred over a simulation were plotted to the right of the kymographs in (Figure 10A-C). In the stationary patterning case (A), it can be seen that the likelihood of differentiating is inhomogeneous. Because low expressing areas are more likely to incur a differentiation event and because these low expression regions are fixed in time, the differentiation distribution reflects the periodicity of the pattern. Conversely, the dynamic spatial pattern and no spatial pattern case (B and C) have more homogeneous spatial distributions of differentiation events, since every cell can switch between higher and lower expression.

To explore how differentiation rate is affected, the distribution of differentiation frequency in individual cells was plotted (Figure 10D-F), along with the differentiation rate of the population as a percentage. The stationary pattern had the highest rate of differentiation at $5.5\%/h$ (D), and the distribution of differentiation frequency in individual cells showed a bimodal distribution, which reflects the two different rates of differentiation occurring in the low and high expressing cells. The dynamic pattern showed a slightly lower rate of differentiation compared to the stationary pattern at $3.9\%/h$, and the distribution has a single peak. The uncoupled no pattern case showed a very low rate of differentiation rate at $0.7\%/h$, and also with a single peak. See Supplementary Movie 1&2 for animated 1D simulations without and with DBP included.

The spatial and temporal measures taken together indicate that for a dynamic pattern, differentiation events are spread out spatially rather than concentrated in one position as is the case in stationary patterns. This spatial spreading of differentiation is also naturally achieved in the case when there is no coupling/no LI, however in the absence of Notch amplifying the differences between cells, cells do not have such a high amplitude between high and low expression, resulting in a much lower rate of differentiation. Therefore dynamic patterning maintains a high differentiation rate like that in stationary patterning, but enables a more homogeneous distribution of differentiating cells in space.

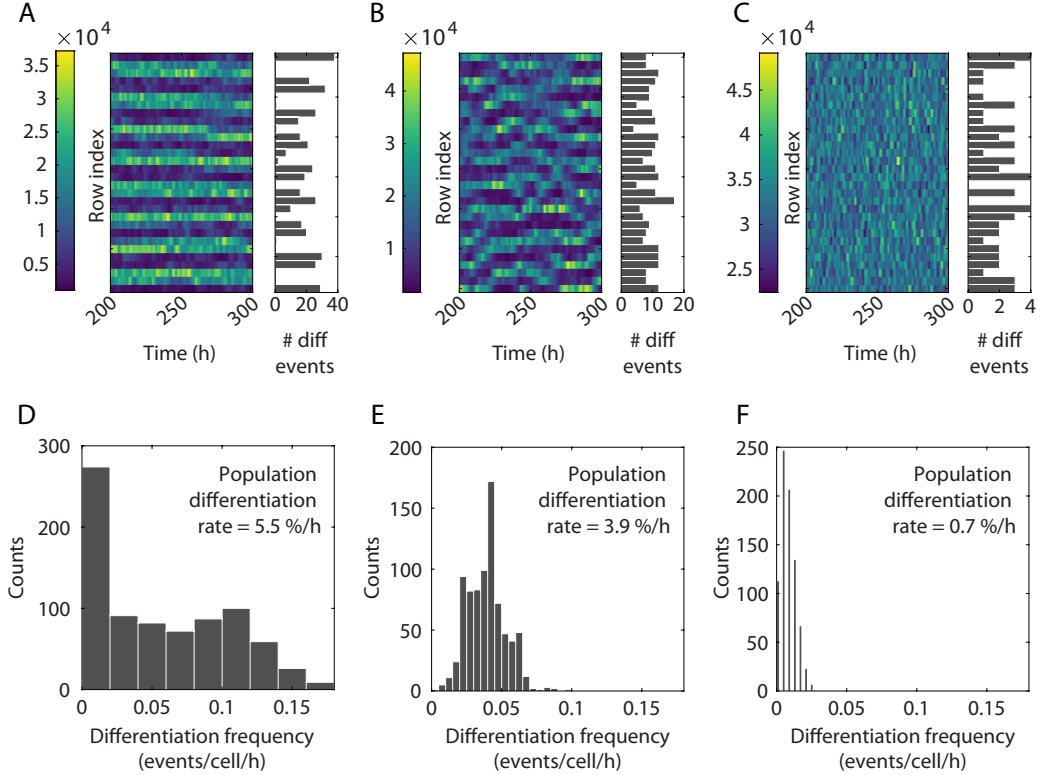


Figure 10: Spatial and temporal measurements of differentiation in three different simulation conditions: **A** and **D** show output from a stationary spatial pattern (no DBP algorithm used), **B** and **E** show a dynamic spatial pattern (DBP algorithm included), **C** and **F** show no spatial pattern (uncoupled cells/no lateral inhibition). **A-C** show the last 100h of simulation as kymographs and plotted to the right of each kymograph is a histogram showing the total number of differentiation events that occur in each row over the entire 300h, though only the last 100h is plotted in the kymographs. **D-F** Histograms of the differentiation frequency (Methods 2.5) in individual cells (events/cell/h), and also the rate of differentiation of the population is given as the a percentage of the population size per hour (800h of simulation to produce graphs **D-F**). All simulation conditions use $P_{ND0} = 3500$, $\frac{\varepsilon_d}{\varepsilon_p} = 1.5$, with a grid size of 26 columns by 1 row.

4 Discussion

In this paper we have investigated the mechanism and function of dynamic spatial patterns in development, motivated by observations of periodic clusters of HES5 expression that change peak and trough location over time [2]. We introduced two methods that can be used to identify dynamic spatial patterns. First, spatial signals at individual time points can be tested for periodicity using a Fisher g -test on the generated power spectra. Second, we proposed the dynamicity coefficient as a measure to test whether peaks and troughs in a spatial signal switch states over time by comparing proportions of time spent in high and low states. Previous models accounted for the observed synchronisation of ultradian oscillations between neighbouring cells, but did not capture the generation of 3-4 cell periodicity or the dynamic switching of the spatial pattern.

To address the generation of a 3-4 cell spatial period, we extended the signalling distance in the model by introducing distal cells (Figure 6D), which generated 3-4 cell periodicity, compared to the 2-cell periodicity that occurs in nearest neighbour signalling. We propose that dynamically extending and retracting protrusions carrying Notch ligands likely account

for extended signalling in the neural tube tissue [17, 25, 26, 27, 28]. If protrusions are the underlying mechanism, then distal signalling efficiency is interpreted as the amount of Notch signalling occurring at the cell body versus at the protrusions. The model predicts that the type of dynamic pattern observed in the neural tube is more likely to occur at higher distal strengths ($\frac{\varepsilon_d}{\varepsilon_p} > 1$). As discussed in section 3.3, this could be due to differences in mechanical activation, diffusion rates, or cis-inhibition between the cell body and the protrusions [48, 18]. Future experimental work should focus around characterising the extent and dynamics of protrusions in the developing mouse neural tube, and where Notch and Delta are localised on cell membranes to get a better picture of where Notch signalling is most active.

To understand how dynamic switching of the spatial pattern arises in the neural tube, we explored the potential role of differentiation and dynamic signalling strength. To translate the differentiation process into the model we implemented a perturbation process where cells that contact a differentiating cell experience an upregulation in HES5 transcription rate (DBP algorithm, outlined in Section 2.5). The inclusion of DBP in the model resulted in a region of parameter space being identified where dynamic spatial patterning occurs, indicating that with sufficient and regular perturbation, high and low states generated by the underlying Notch LI circuit can be dynamically switched and reorganised. Additionally, nested dynamics of ultradian oscillations on top of the larger-amplitude switching dynamics were observed in the model-generated single-cell time traces (Figure 9), similar to that observed *ex vivo* [2]. One aspect that remains unclear due to experimental limits of the observation time of the *ex vivo* slices, is the regularity of switching. Future experimental work therefore would be very informative if longer observation times could be obtained, as this would enable more detailed comparison of the model generated persistence time distributions against the data.

Due to higher numbers of signalling interactions in the 2D simulations, regions of dynamic patterning in parameter space were found to be more restricted than in the 1D simulations. From biological studies, the average number of signalling neighbours per RG cell is not known, so whether the 1D or 2D simulations are more representative of the biological system is unclear. Some studies suggest that most of the Notch signalling occurs at the apical side of the neuroepithelium [29, 49] in which case the restricted number of spatial interactions might be more akin to the 1D model. Other studies show that Delta-carrying protrusions extend down from the basally located newborn neurons to interact with apically located RG cells, and RG cells extend dynamic protrusions in both apical and non-apical locations, in which case the 2D simulations may be more representative of the number of signalling interactions [25, 26, 28]. An additional consideration is where and when differentiating cells have an altered signalling effect on their neighbours. It would be interesting to introduce cell movement into future modelling so as to investigate the effect of the apical-basal migration of differentiating cells.

It is important to consider that perturbations could reasonably come from sources other than altered signalling in differentiating cells. Processes such as the extension and retraction of signalling protrusions, cell cycle variations in HES5/coupling strength, interkinetic nuclear migration, and pulsatile Dll1 signalling are all reasonable candidates in contributing to the switching behaviour [50, 25, 51, 52, 28]. The DBP algorithm is general enough that it could reasonably be adapted to any of the listed alternatives, by altering the magnitude and duration of the perturbation, as well as the parameter it is applied to. Furthermore, there are also entirely separate mechanisms that could underlie the observed HES5 pattern that are not perturbation based. For example, we also explored morphogen gradient induced travelling waves as a potential mechanism (not included in this study), inspired by somitogenesis studies. We found the travelling waves did not as closely match the data and required assumptions that seemed less likely from the literature, but we cannot rule this mechanism out without further exploration. For the mechanism underlying the clustered/extended spatial periodicity, it may be also worth considering modifications of Notch signalling such as cis-inhibition or lateral induction from other Notch ligands such as Jagged, as both of these mechanisms show a tendency to form longer range or clustered patterning [53, 54].

Regardless of underlying mechanisms, this is a model that produces a dynamic pattern suffi-

ciently similar to that of HES5 in the neural tube and so we tested what functional advantage such a dynamic pattern might provide during development, finding that dynamic patterning spreads out differentiation events spatially, rather than generating hotspots of differentiation like in the stationary case. Stationary patterning seems most suited to tissues where differentiating cells remain within the progenitor population and need to be regularly spaced apart such as in the formation of sensory hairs in *Drosophila* [19]. In the developing neural tube, differentiating cells do not form a regular pattern of differentiated cells within the progenitor population itself, rather they leave the progenitor population and migrate basally to form neurons and glia at later stages [55]. Though the functional advantage of dynamic patterning is not established, we conjecture that it ensures that the production of neurons is evenly distributed across the dorsal-ventral axis, and prevents many differentiating cells from being repeatedly produced in the same locations as in the stationary patterning case.

In sum, we have explored how a stationary pattern generating signalling network, Notch LI, can be made dynamic through the introduction of perturbations that enable cells to switch between high and low expression. We suggest that a combination of protrusions and altered signalling strength coming from differentiating cells are the most likely underlying mechanisms that produce the dynamic HES5 spatial pattern found in the developing neural tube. However, further experiments need to be carried out regarding the presence of Notch carrying protrusions, and whether these protrusions are capable of generating extended periodicity, along with tests of how much perturbation comes from differentiating cells in the developing neural tube.

Data availability

All code is written in MATLAB and is available at <https://github.com/Papalopulu-Lab/Hawley2022>.

Acknowledgements

Joshua Hawley was supported by a Wellcome Trust PhD studentship (220001/Z/19/Z). The funders had no role in study design, data collection and analysis, decision to publish, or preparation of the manuscript.

References

- [1] Cerys S Manning, Veronica Biga, James Boyd, Jochen Kursawe, Bodvar Ymisson, David G Spiller, Christopher M Sanderson, Tobias Galla, Magnus Rattray, and Nancy Papalopulu. Quantitative single-cell live imaging links hes5 dynamics with cell-state and fate in murine neurogenesis. *Nature communications*, 10(1):1–19, 2019.
- [2] Veronica Biga, Joshua Hawley, Ximena Soto, Emma Johns, Daniel Han, Hayley Bennett, Antony D Adamson, Jochen Kursawe, Paul Glendinning, Cerys S Manning, et al. A dynamic, spatially periodic, micro-pattern of hes5 underlies neurogenesis in the mouse spinal cord. *Molecular systems biology*, 17(5):e9902, 2021.
- [3] Magdalena Götz and Wieland B Huttner. The cell biology of neurogenesis. *Nature reviews Molecular cell biology*, 6(10):777–788, 2005.
- [4] Raman M Das and Kate G Storey. Apical abscission alters cell polarity and dismantles the primary cilium during neurogenesis. *Science*, 343(6167):200–204, 2014.
- [5] Jun Hatakeyama, Yasumasa Bessho, Kazuo Katoh, Shigeo Ookawara, Makio Fujioka, François Guillemot, and Ryoichiro Kageyama. Hes genes regulate size, shape and histogenesis of the nervous system by control of the timing of neural stem cell differentiation. *Development*, 2004.

- [6] Hiromi Shimojo, Toshiyuki Ohtsuka, and Ryoichiro Kageyama. Oscillations in notch signaling regulate maintenance of neural progenitors. *Neuron*, 58(1):52–64, 2008.
- [7] Verónica Martínez-Cerdeño and Stephen C Noctor. Neural progenitor cell terminology. *Frontiers in neuroanatomy*, 12:104, 2018.
- [8] Andreas Sagner, Zachary B Gaber, Julien Delile, Jennifer H Kong, David L Rousso, Caroline A Pearson, Steven E Weicksel, Manuela Melchionda, S Neda Mousavy Gharavy, James Briscoe, et al. Olig2 and hes regulatory dynamics during motor neuron differentiation revealed by single cell transcriptomics. *PLoS biology*, 16(2):e2003127, 2018.
- [9] Ryoichiro Kageyama, Hiromi Shimojo, and Toshiyuki Ohtsuka. Dynamic control of neural stem cells by bhlh factors. *Neuroscience research*, 138:12–18, 2019.
- [10] Emma R Andersson, Rickard Sandberg, and Urban Lendahl. Notch signaling: simplicity in design, versatility in function. *Development*, 138(17):3593–3612, 2011.
- [11] Kristina Preuße, Lena Tveriakhina, Karin Schuster-Gossler, Cláudia Gaspar, Alexandra Isabel Rosa, Domingos Henrique, Achim Gossler, and Michael Stauber. Context-dependent functional divergence of the notch ligands dll1 and dll4 in vivo. *PLoS genetics*, 11(6):e1005328, 2015.
- [12] Ulrika Marklund, Emil M Hansson, Erik Sundström, Martin Hrabé de Angelis, Gerhard KH Przemeck, Urban Lendahl, Jonas Muhr, and Johan Ericson. Domain-specific control of neurogenesis achieved through patterned regulation of notch ligand expression. *Development*, 137(3):437–445, 2010.
- [13] Eva Kutejova, Noriaki Sasai, Ankita Shah, Mina Gouti, and James Briscoe. Neural progenitors adopt specific identities by directly repressing all alternative progenitor transcriptional programs. *Developmental cell*, 36(6):639–653, 2016.
- [14] Itaru Imayoshi and Ryoichiro Kageyama. Oscillatory control of bhlh factors in neural progenitors. *Trends in neurosciences*, 37(10):531–538, 2014.
- [15] Marc AT Muskavitch. Delta-notch signaling and drosophila cell fate choice. *Developmental biology*, 166(2):415–430, 1994.
- [16] Joanne R Collier, Nicholas AM Monk, Philip K Maini, and Julian H Lewis. Pattern formation by lateral inhibition with feedback: a mathematical model of delta-notch intercellular signalling. *Journal of theoretical Biology*, 183(4):429–446, 1996.
- [17] Michael Cohen, Marios Georgiou, Nicola L Stevenson, Mark Miodownik, and Buzz Baum. Dynamic filopodia transmit intermittent delta-notch signaling to drive pattern refinement during lateral inhibition. *Developmental cell*, 19(1):78–89, 2010.
- [18] Zena Hadjivasiliou, Ginger L Hunter, and Buzz Baum. A new mechanism for spatial pattern formation via lateral and protrusion-mediated lateral signalling. *Journal of the Royal Society Interface*, 13(124):20160484, 2016.
- [19] Francis Corson, Lydie Couturier, Hervé Rouault, Khalil Mazouni, and François Schweiguth. Self-organized notch dynamics generate stereotyped sensory organ patterns in drosophila. *Science*, 356(6337), 2017.
- [20] Lydie Couturier, Khalil Mazouni, Francis Corson, and François Schweiguth. Regulation of notch output dynamics via specific e (spl)-hlh factors during bristle patterning in drosophila. *Nature communications*, 10(1):1–13, 2019.
- [21] Federico Bocci, José Nelson Onuchic, and Mohit Kumar Jolly. Understanding the principles of pattern formation driven by notch signaling by integrating experiments and theoretical models. *Frontiers in Physiology*, page 929, 2020.

- [22] Hiromi Shimojo, Akihiro Isomura, Toshiyuki Ohtsuka, Hiroshi Kori, Hitoshi Miyachi, and Ryoichiro Kageyama. Oscillatory control of delta-like1 in cell interactions regulates dynamic gene expression and tissue morphogenesis. *Genes & development*, 30(1):102–116, 2016.
- [23] Hendrik B Tiedemann, Elida Schneltzer, Johannes Beckers, Gerhard KH Przemeck, and Martin Hrabě de Angelis. Modeling coexistence of oscillation and delta/notch-mediated lateral inhibition in pancreas development and neurogenesis. *Journal of Theoretical Biology*, 430:32–44, 2017.
- [24] Cyrille De Joussineau, Jonathan Soule, Marianne Martin, Christelle Anguille, Philippe Montcourrier, and Daniel Alexandre. Delta-promoted filopodia mediate long-range lateral inhibition in drosophila. *Nature*, 426(6966):555–559, 2003.
- [25] Branden R Nelson, Rebecca D Hodge, Francesco Bedogni, and Robert F Hevner. Dynamic interactions between intermediate neurogenic progenitors and radial glia in embryonic mouse neocortex: potential role in dll1-notch signaling. *Journal of Neuroscience*, 33(21):9122–9139, 2013.
- [26] Zena Hadjivassiliou, Rachel E Moore, Rebecca McIntosh, Gabriel L Galea, Jonathan DW Clarke, and Paula Alexandre. Basal protrusions mediate spatiotemporal patterns of spinal neuron differentiation. *Developmental cell*, 49(6):907–919, 2019.
- [27] Rachel E Moore, Jon Clarke, and Paula Alexandre. Protrusion-mediated signaling regulates patterning of the developing nervous system. *Frontiers in Cell and Developmental Biology*, 8, 2020.
- [28] Ioannis Kasioulis, Alwyn Dady, John James, Alan Prescott, Pamela A Halley, and Kate G Storey. A lateral protrusion latticework connects neuroepithelial cells and is regulated during neurogenesis. *Journal of Cell Science*, 135(6):jcs259897, 2022.
- [29] Jun Hatakeyama, Yoshio Wakamatsu, Akira Nagafuchi, Ryoichiro Kageyama, Ryuichi Shigemoto, and Kenji Shimamura. Cadherin-based adhesions in the apical endfoot are required for active notch signaling to control neurogenesis in vertebrates. *Development*, 141(8):1671–1682, 2014.
- [30] Bon-Kyoung Koo, Hyoung-Soo Lim, Ran Song, Mi-Jeong Yoon, Ki-Jun Yoon, Jin-Sook Moon, Young-Woong Kim, Min-chul Kwon, Kyeong-Won Yoo, Myung-Phil Kong, et al. Mind bomb 1 is essential for generating functional notch ligands to activate notch. *Development*, 132(15):3459–3470, 2005.
- [31] Ki-Jun Yoon, Bon-Kyoung Koo, Sun-Kyoung Im, Hyun-Woo Jeong, Jaewang Ghim, Min-chul Kwon, Jin-Sook Moon, Takaki Miyata, and Young-Yun Kong. Mind bomb 1-expressing intermediate progenitors generate notch signaling to maintain radial glial cells. *Neuron*, 58(4):519–531, 2008.
- [32] Chooyoung Baek, Lucy Freem, Rosette Goiame, Helen Sang, Xavier Morin, and Samuel Tozer. Mib1 prevents notch cis-inhibition to defer differentiation and preserve neuroepithelial integrity during neural delamination. *PLoS biology*, 16(4):e2004162, 2018.
- [33] Laurence Meloty-Kapella, Bhupinder Shergill, Jane Kuon, Elliot Botvinick, and Gerry Weinmaster. Notch ligand endocytosis generates mechanical pulling force dependent on dynamin, epsins, and actin. *Developmental cell*, 22(6):1299–1312, 2012.
- [34] Nicholas AM Monk. Oscillatory expression of hes1, p53, and nf- κ b driven by transcriptional time delays. *Current Biology*, 13(16):1409–1413, 2003.
- [35] Daniel T Gillespie. The chemical langevin equation. *The Journal of Chemical Physics*, 113(1):297–306, 2000.

- [36] Julian Lewis. Autoinhibition with transcriptional delay: a simple mechanism for the zebrafish somitogenesis oscillator. *Current Biology*, 13(16):1398–1408, 2003.
- [37] Leah Herrgen, Saúl Ares, Luis G Morelli, Christian Schröter, Frank Jülicher, and Andrew C Oates. Intercellular coupling regulates the period of the segmentation clock. *Current Biology*, 20(14):1244–1253, 2010.
- [38] Akihiro Isomura, Fumiko Ogushi, Hiroshi Kori, and Ryoichiro Kageyama. Optogenetic perturbation and bioluminescence imaging to analyze cell-to-cell transfer of oscillatory information. *Genes & development*, 31(5):524–535, 2017.
- [39] Joseph W Baron and Tobias Galla. Intrinsic noise, delta-notch signalling and delayed reactions promote sustained, coherent, synchronized oscillations in the presomitic mesoderm. *Journal of the Royal Society Interface*, 16(160):20190436, 2019.
- [40] Kumiko Yoshioka-Kobayashi, Marina Matsumiya, Yusuke Niino, Akihiro Isomura, Hiroshi Kori, Atsushi Miyawaki, and Ryoichiro Kageyama. Coupling delay controls synchronized oscillation in the segmentation clock. *Nature*, 580(7801):119–123, 2020.
- [41] Sofia Wichert, Konstantinos Fokianos, and Korbinian Strimmer. Identifying periodically expressed transcripts in microarray time series data. *Bioinformatics*, 20(1):5–20, 2004.
- [42] Alan Wee-Chung Liew, Ngai-Fong Law, Xiao-Qin Cao, and Hong Yan. Statistical power of fisher test for the detection of short periodic gene expression profiles. *Pattern Recognition*, 42(4):549–556, 2009.
- [43] Ronald W Schafer. What is a savitzky-golay filter?[lecture notes]. *IEEE Signal processing magazine*, 28(4):111–117, 2011.
- [44] Ayano Kawaguchi. Neuronal delamination and outer radial glia generation in neocortical development. *Frontiers in Cell and Developmental Biology*, page 1883, 2021.
- [45] Georgios Vasilopoulos and Kevin J Painter. Pattern formation in discrete cell tissues under long range filopodia-based direct cell to cell contact. *Mathematical Biosciences*, 273:1–15, 2016.
- [46] Supriya Bajpai, Ranganathan Prabhakar, Raghunath Chelakkot, and Mandar M Inamdar. Role of cell polarity dynamics and motility in pattern formation due to contact-dependent signalling. *Journal of the Royal Society Interface*, 18(175):20200825, 2021.
- [47] Barbara Hä默le and Francisco J Tejedor. A novel function of delta-notch signalling mediates the transition from proliferation to neurogenesis in neural progenitor cells. *PloS one*, 2(11):e1169, 2007.
- [48] Itzhak Khait, Yuval Orsher, Ohad Golan, Udi Binshtok, Nadav Gordon-Bar, Liat Amir-Zilberstein, and David Sprinzak. Quantitative analysis of delta-like 1 membrane dynamics elucidates the role of contact geometry on notch signaling. *Cell reports*, 14(2):225–233, 2016.
- [49] Erin Banda, Anna McKinsey, Noelle Germain, James Carter, Nickesha Camille Anderson, and Laura Grabel. Cell polarity and neurogenesis in embryonic stem cell-derived neural rosettes. *Stem cells and development*, 24(8):1022–1033, 2015.
- [50] Philip C Spear and Carol A Erickson. Interkinetic nuclear migration: a mysterious process in search of a function. *Development, growth & differentiation*, 54(3):306–316, 2012.
- [51] Nagarajan Nandagopal, Leah A Santat, Lauren LeBon, David Sprinzak, Marianne E Bronner, and Michael B Elowitz. Dynamic ligand discrimination in the notch signaling pathway. *Cell*, 172(4):869–880, 2018.

- [52] Nitin Sabherwal, Andrew Rowntree, Elli Marinopoulou, Tom Pettini, Sean Hourihane, Riba Thomas, Ximena Soto, Jochen Kursawe, and Nancy Papalopulu. Differential phase register of hes1 oscillations with mitoses underlies cell-cycle heterogeneity in er+ breast cancer cells. *Proceedings of the National Academy of Sciences*, 118(45), 2021.
- [53] Markus R Owen, Jonathan A Sherratt, and Helen J Wearing. Lateral induction by juxtacrine signaling is a new mechanism for pattern formation. *Developmental biology*, 217(1):54–61, 2000.
- [54] Pau Formosa-Jordan and Marta Ibañes. Competition in notch signaling with cis enriches cell fate decisions. *PloS one*, 9(4):e95744, 2014.
- [55] Judith TML Paridaen and Wieland B Huttner. Neurogenesis during development of the vertebrate central nervous system. *EMBO reports*, 15(4):351–364, 2014.

Supplementary

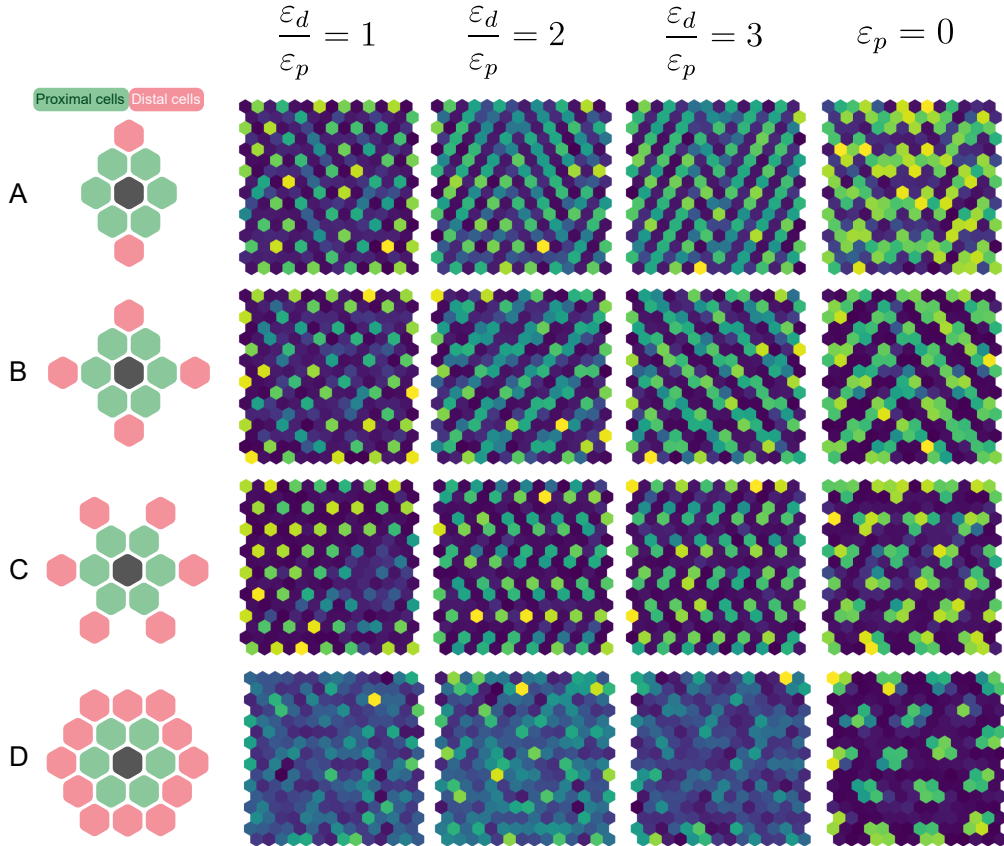


Figure S1: Exploration of different distal cell geometries. Each row (**A-D**) corresponds to a different geometry and each column correspond to a different distal signalling efficiency with the last column showing the model output when no proximal cells are included. Simulations were run stochastically for 300h and the final time point is shown. A repression threshold value of $P_{0,LI} = 4000$ was used for all simulations.

1D simulation

DBP algorithm perturbation time

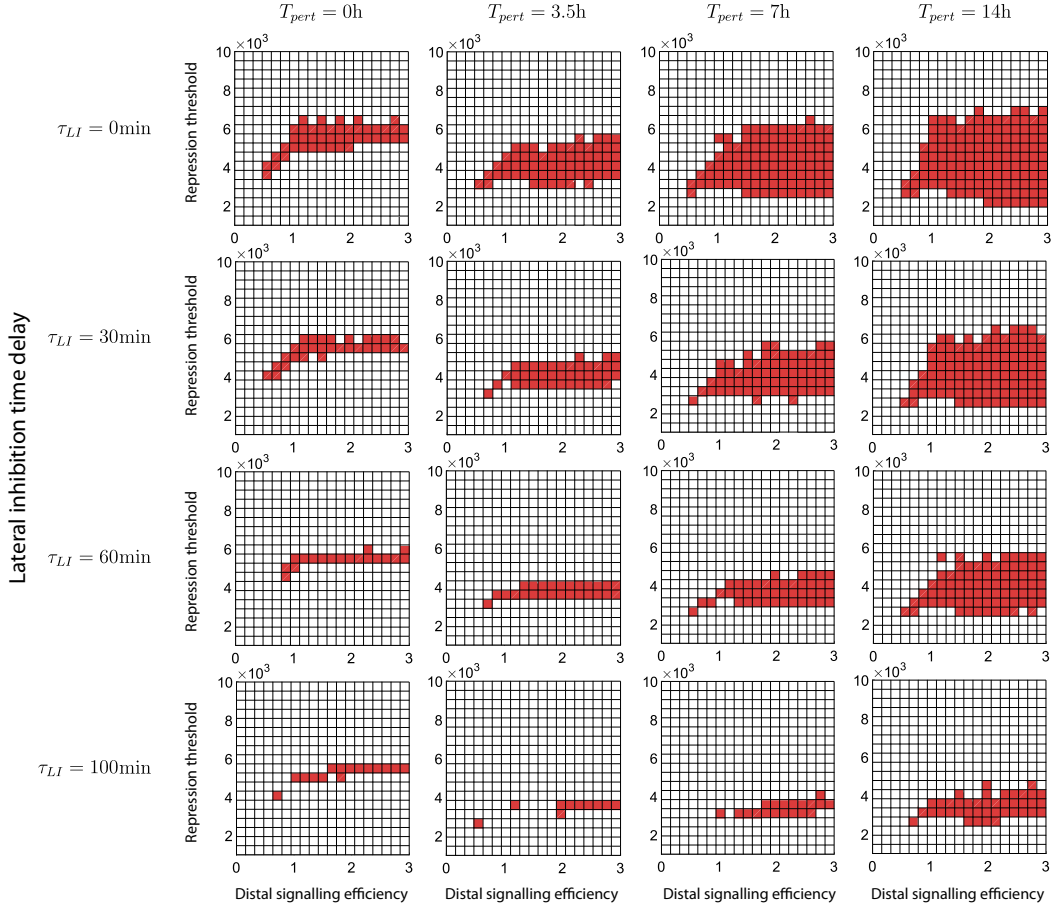


Figure S2: Effect of lateral inhibition time delay, τ_{LI} , and differentiation time, T_{pert} , on the region of dynamic patterning (red) in 1D simulations (simulation final time 200h, 20 repeats, 26 row, 1 column).

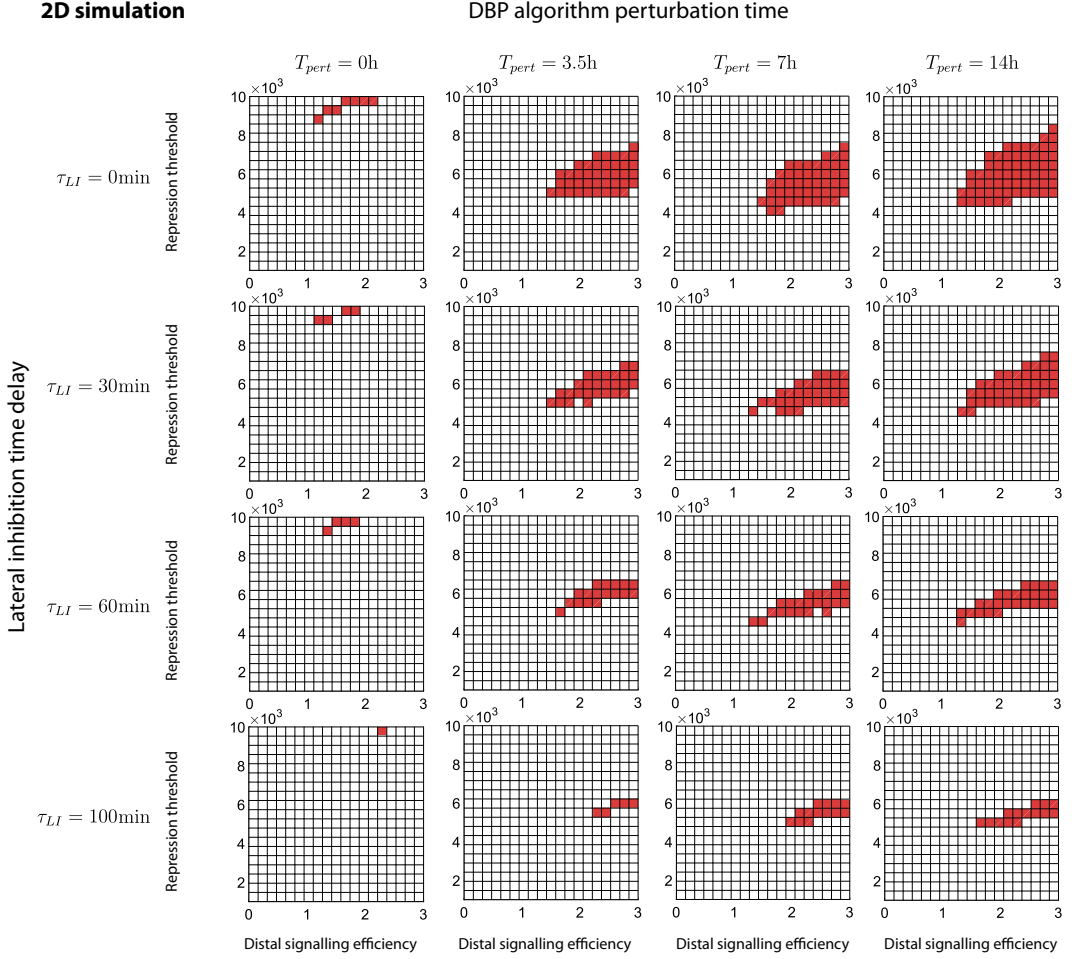


Figure S3: Effect of lateral inhibition time delay, T_{LI} , and differentiation time, T_{pert} , on the region of dynamic patterning (red) in 2D simulations (simulation final time 200h, 20 repeats, 26 row, 6 columns).

Supplementary movie captions

Supplementary Movie 1: 1D simulation of 26 rows by 1 column with no DBP algorithm included. A rolling kymograph is shown, as is the HES5 expression in the hexagonal lattice. Locations of differentiating cells are recorded but these do not change the signalling in neighbouring cells. The bar chart shows the total number of differentiation events recorded on each row. Simulation used $P_{0,LI} = 3500$, $\frac{\varepsilon_d}{\varepsilon_p} = 1.5$, simulation run time of 500h.

Supplementary Movie 2: 1D simulation of 26 rows by 1 column that does include the DBP algorithm. A rolling kymograph is shown, as is the HES5 expression in the hexagonal lattice. Locations of differentiating cells are recorded which alter the signalling in the neighbouring cells. The bar chart shows the total number of differentiation events recorded on each row. Simulation used $P_{0,LI} = 3500$, $\frac{\varepsilon_d}{\varepsilon_p} = 2$, $F_{pert} = 3$, $T_{pert} = 7h$, simulation run time of 500h.

Supplementary Movie 3: 2D simulation of 26 rows by 6 columns that does include the DBP algorithm. A rolling kymograph is shown which is plotting the expression in the first column of the simulated grid. HES5 expression in the hexagonal lattice is shown also. Locations of differentiating cells are recorded which alter the signalling in the neighbouring cells. Simulation used $P_{0,LI} = 6000$, $\frac{\varepsilon_d}{\varepsilon_p} = 2$, $F_{pert} = 3$, $T_{pert} = 7h$, simulation run time of 500h.